

PHOTOSYSTEM II-BASED BIOSENSOR FOR THE
DETECTION OF EXPLOSIVE COMPOUNDS

ZHAO XIN

A THESIS
IN
THE DEPARTMENT
OF
CHEMISTRY AND BIOCHEMISTRY

PRESENTED IN PARTIAL FULFILLMENT OF THE REQUIREMENTS
FOR THE DEGREE OF MASTER OF SCIENCE
CONCORDIA UNIVERSITY
MONTRÉAL, QUÉBEC, CANADA

SEPTEMBER 2010
© ZHAO XIN, 2010



Library and Archives
Canada

Published Heritage
Branch

395 Wellington Street
Ottawa ON K1A 0N4
Canada

Bibliothèque et
Archives Canada

Direction du
Patrimoine de l'édition

395, rue Wellington
Ottawa ON K1A 0N4
Canada

Your file *Votre référence*
ISBN: 978-0-494-80153-6
Our file *Notre référence*
ISBN: 978-0-494-80153-6

NOTICE:

The author has granted a non-exclusive license allowing Library and Archives Canada to reproduce, publish, archive, preserve, conserve, communicate to the public by telecommunication or on the Internet, loan, distribute and sell theses worldwide, for commercial or non-commercial purposes, in microform, paper, electronic and/or any other formats.

The author retains copyright ownership and moral rights in this thesis. Neither the thesis nor substantial extracts from it may be printed or otherwise reproduced without the author's permission.

In compliance with the Canadian Privacy Act some supporting forms may have been removed from this thesis.

While these forms may be included in the document page count, their removal does not represent any loss of content from the thesis.

AVIS:

L'auteur a accordé une licence non exclusive permettant à la Bibliothèque et Archives Canada de reproduire, publier, archiver, sauvegarder, conserver, transmettre au public par télécommunication ou par l'Internet, prêter, distribuer et vendre des thèses partout dans le monde, à des fins commerciales ou autres, sur support microforme, papier, électronique et/ou autres formats.

L'auteur conserve la propriété du droit d'auteur et des droits moraux qui protège cette thèse. Ni la thèse ni des extraits substantiels de celle-ci ne doivent être imprimés ou autrement reproduits sans son autorisation.

Conformément à la loi canadienne sur la protection de la vie privée, quelques formulaires secondaires ont été enlevés de cette thèse.

Bien que ces formulaires aient inclus dans la pagination, il n'y aura aucun contenu manquant.


Canada

Abstract

Photosystem II-Based Biosensor for the Detection of Explosive Compounds

Zhao Xin

Research on herbicide biosensors based on plant photosystem II (PS II) or on reaction centers of purple bacteria (BRC) has been on-going for the past decade. Herbicides inhibit functioning of the PS II by competitively binding to the Q_B plastoquinone binding site. The structural similarity between nitric explosives and nitrophenolic- and atrazine-type herbicides inspired us to explore whether nitric explosives would inhibit photosynthesis via the same mechanism (involving Q_B site) as the herbicides. The design of the explosives biosensor was similar to that of the biosensors for herbicides. The detection was achieved by photo-electrochemical methods, employing PS II immobilized on a screen-printed electrode as a part of electrical circuit; optical spectroscopy was used as a supplementary method. We have demonstrated that this electrochemical biosensor is capable of detecting explosives such as picric acid, TNT and tetryl. The magnitude of the peak current induced by illumination depends on the concentration of the explosive in the same manner as in the case of herbicides, which suggests that Q_B binding site is indeed involved in the PS II inhibition of the selected explosive compounds. However, the limits of detection for explosives, especially for TNT, appear to be higher (i.e. worse) than for the herbicides. Modeling of photosynthesis inhibitor docking on PS II has also been performed to determine the reasons for poor TNT detection.

Acknowledgments

This work is dedicated to my parents in China. Without their encouragement and support it would have been impossible for me to finish this work.

I would like to express my deep and sincere gratitude to my supervisor, Dr. Valter Zazubovits. His wide knowledge and his logical way of thinking have been of great value for me. His understanding, encouraging and personal guidance have provided a good basis for the present thesis.

I also owe my most sincere gratitude to Dr. Vijayender Bhalla, who has started his new research career in India. His professional knowledge in the field and patient help was of crucial importance during my whole study.

I am happy to acknowledge my friends in Concordia University: Sasmit Deshmukh, Zhuo Xuan Yang, Beste Korutlu and Nicoleta Herascu for their helpful discussions and comments.

Finally, I want to thank the Canada Foundation for Innovation and NSERC for their financial support.

Contents

List of Figures	vii
List of Tables	ix
List of Abbreviations	x
1 Introduction	1
2 Photosystem II	6
2.1 Basic principles of photosynthesis	6
2.2 Structure of PS II complex	9
2.3 Isolation of PS II	16
2.4 Electron transfer process in the PS II complex	18
2.5 Quinone binding site in PS II	20
2.6 Binding of the inhibitors at the Q_B site	23
3 Material and Method	28
3.1 Preparation of PS II samples	28
3.1.1 Purification of thylakoid membranes	28
3.1.2 Purification of BBY Membranes	30
3.2 DCPIP assay	31
3.2.1 Photosynthetic activity	32
3.2.2 Effect of PS II inhibitors on DCPIP measurement	33
3.3 Immobilization of PS II particles for the biosensor	33
3.4 Photo-electrochemical measurements	34
3.5 Analysis of inhibitor binding	38
3.6 Components of buffers	39

4	Detection of explosives/herbicides with biosensor	40
4.1	Principle of detection using biosensor	40
4.2	Characteristics of the PS II membranes	42
4.3	Optimization of biosensor activity	47
4.4	Results of detection with the biosensor	50
4.5	Supplemental studies of TNT	55
5	Molecular modeling of inhibitors binding to PS II	60
5.1	Introduction to Autodock	60
5.2	Docking of inhibitors by AutoDock Vina	62
5.2.1	Docking of Plastoquinone	63
5.2.2	Docking of explosive molecules	65
5.2.3	Docking of herbicide molecules	69
5.2.4	Discussion of docking results by AutoDock	71
6	Conclusion	74
	Bibliography	76

List of Figures

2.1.1 The Z-scheme of oxygenic photosynthesis	7
2.1.2 The overall reaction of PS II	8
2.2.1 Organization of protein complexes in thylakoid membranes	9
2.2.2 Overall Structure of PS II core complex	14
2.3.1 Thylakoid structures	16
2.3.2 Different chlorophyll containing bands in different components of thylakoid membrane	17
2.4.1 PS II primary electron transport and oxygen evolution	18
2.5.1 PS II RC cofactors involved in electron transfer	21
2.5.2 Electron acceptors of PS II	22
2.6.1 Schematic figure of the plastoquinone/herbicide binding pocket of the D1 protein	25
2.6.2 Displacement of Q_B by inhibitors	25
2.6.3 Herbicides as PS II inhibitors and explosives as potential inhibitors .	27
3.2.1 The reduction of DCPIP	31
3.4.1 Theoretical cyclic voltammogram	36
3.4.2 Scheme of amperometric readout upon increasing the concentration of the inhibitors.	38
4.1.1 Photocurrent signals of DCMU detection	42
4.2.1 UV-Vis spectra of PS II particles during preparations	43
4.2.2 Photo-current signals of biosensor employing (A) thylakoid membrane and (B)BBY membrane	45
4.3.1 Wavelength dependence of photocurrent signals of the BBY-based biosensor	48
4.3.2 Time dependence of stability of the biosensor	49
4.4.1 Binding curves of DCMU and explosives in the presence of 0.2mM DQ	51

4.5.1 Binding curves of TNT in the presence of 1mM FeCy	55
4.5.2 Binding curve of TNT-DCPIP assay	56
4.5.3 Recoverability of biosensor after the detection of TNT	58
5.2.1 Model of binding site of PQ in the Q _B pocket by Takahashi et al. . .	63
5.2.2 Binding of PQ in the Q _B pocket of PS II	64
5.2.3 Binding of picric acid in the Q _B pocket of PS II	66
5.2.4 Two models of binding of TNT on PS II	67
5.2.5 Binding of tetryl in the Q _B pocket of PS II	68
5.2.6 Two models of binding of DCMU in the Q _B pocket	69
5.2.7 Binding of atrazine in the Q _B pocket of PS II	70

List of Tables

2.2.1 The PS II subunits: primary and secondary structure, and function .	10
3.6.1 Components of buffers	39
4.2.1 Chlorophyll content from spectra in Figure 4.2.1	44
4.2.2 Photocurrent signal performance of biosensors immobilized with thylakoid membrane and BBY membrane.	46
4.4.1 Detection results based on binding curves in Figure 4.4.1	52
5.2.1 Modeling results of the PS II inhibitors binding to the Q_B pocket . .	73

List of Abbreviations

ATP	Adenosine triphosphate
BRC	Bacteria reaction center
BSA	Bovine serum albumin
Chl	Chlorophyll
Cyt	Cytochrome
DCMU	3-(3,4-dichlorophenyl)-1,1-dimethylurea
DCPIP	2,6-Dichlorophenolindophenol
DQ	Duroquinone
EC50	Half maximum efficient concentration
FeCy	Ferricyanide
LHC	Light harvesting complex
LOD	Limit of detection
NADP	Nicotinamide adenine dinucleotide phosphate
OEC	Oxygen-evolving center
PDB	Protein Data Bank
PQ	Plastoquinone
PQH ₂	Plastoquinol
PS II	Photosystem II
RDX	Cyclotrimethylenetrinitramine
RMS	Root mean square

SNR

Signal to noise ratio

TNT

Trinitrotoluene

Chapter 1

Introduction

Nitric explosives, e.g. TNT, RDX, and nitrophenols comprise one of the largest classes of explosives and are frequently used by terrorist organizations around the world because of their ease of manufacture and because of their relative accessibility due to the extensive use by the military and commercial enterprises. Various methods for detection of explosives have been developed or proposed. Unfortunately, the most sensitive of them, such as liquid or gas chromatography, are relatively slow and require instrumentation that is too complex and expensive for use in the field. Various other approaches have been recently proposed. For example, quenching of the fluorescence of pyrene [1], Nile Red [2] or semiconductor organic polymers [3] by nitric explosives was described. The last approach is currently being commercialized [4]. Selective detection of explosives using immunosensors is based on the high affinity and selectivity of the analyte/antibody interaction that is detected using either plasmon resonance [5] or changes in the fluorescence or bioluminescence of the reporter proteins incorporated into the antibody [6]. However, antibodies are

difficult to prepare, and are very analyte-specific and have issues of stability in harsh environments. Summarizing, there is an apparent need to continue the development of new methods of detection of explosives, with the long-term objective of making them faster, less expensive, more sensitive and more reliable. One should also note that for the purposes of reducing the number of the false positives, it would be beneficial to introduce systems with several “orthogonal” detection technologies (i.e. utilizing different physical, chemical or biological principles).

In this thesis, we describe development of a droplet biosensor system based on inhibition of Photosystem II (PS II) to sense trace levels of explosive compounds. The idea for such a sensor is inspired by recent progress in the development of inexpensive and sensitive herbicide biosensors based on photosynthetic reaction centers [7, 8]. It is important to note that the chemical structures of nitric explosives are very similar to those of the herbicides detectable by these biosensors; moreover, nitric explosives are known to be strong electron acceptors. Thus, detection of explosives by natural photosynthetic RC-based sensors seems quite promising. PS II is a transmembrane protein complex responsible for the water splitting and oxygen evolution; it is a part of the electron transfer chain in photosynthesis. In PS II optical energy is utilized to cause charge separation starting with the formation of $P680^+$ - $Pheo^-$ pair. The electron then travels from the pheophytine to immobile quinone Q_A and then to mobile quinone Q_B . The latter accepts two electrons (and two protons from water), transforms to hydroquinone and carries the electrons away.

The development of the PS II-based herbicide biosensors has been reported in a

series of papers [9, 10]. The most recent setup of Koblizek et al. [9] employs screen-printed graphite electrodes and PS II from thermophilic cyanobacteria immobilized in a BSA-glutaraldehyde matrix [9]. The mechanism of inhibition of photosynthetic reaction centers by herbicides involves herbicide molecules attaching to the Q_B binding site of the mobile plastoquinone electron acceptor and preventing the latter from binding. The exposure of the sensor to the inhibitor results in a decrease of the photoinduced current in an electrical circuit containing the photosynthetic reaction centers. The photocurrent signal is registered by potential control method so that the inhibition ability can be quantized.

Detection of TNT, picric acid and tetryl will be considered in this study. Picric acid, or 2,4,6-trinitrophenol, one of the most acidic phenols, is a yellow crystalline solid, easily soluble in water. Like other highly nitrated compounds such as TNT, picric acid is an explosive which was widely employed during the World War I. It is also used for various laboratory purposes, such as staining biological samples and preservation of specimens. On exposure to metals picric acid forms picrate salts which are even more sensitive than the picric acid itself. Some optical sensors for the detection of picric acid have been reported [11, 12, 13, 14]. Some evidence of picric acid being an inhibitor of photosynthetic electron transport in PS II has been reported a while ago [15].

TNT is used in organic synthesis but is best known as an explosive material with convenient handling properties. Among the commonly used methods for detection of TNT are spectrophotometric [16, 17], immunoassay [18, 5] and electrochemical [19].

TNT is a strong electron acceptor and this very property has been used recently for detection purposes employing quenching of photoluminescence of polysiloles [20]. The solubility of TNT in water varies from 100 to 200 mg/L at room temperature [21]. It is readily taken up by plant roots from the soil [22] and it is known to inhibit the growth of the plants [23].

2,4,6-Trinitrophenylmethylnitramine (commonly referred to as tetryl) is a sensitive explosive compound used to make detonators and explosive booster charges. Because of its extreme thermal and base lability as well as its propensity to undergo photodecomposition in water and soil extracts [24], an appropriate analytical methodology needs to be developed which is rapid and accurate. HPLC was applied in analyzing of the metabolism of tetryl in plant by Harvey et al [25]. The early research reported that nitrite group on tetryl could be eliminated by ferredoxin NADP oxidoreductase [26]. Hodyss and Beauchamp [27] used a multidimensional GC-Pyrolysis-Ultraviolet system to detect nitroorganic explosives and reported a detection limit of 50 ng for tetryl.

At the beginning of this thesis we will review the background information on Photosystem II , i.e. the protein structure, the photosynthetic function, the preparation method and the inhibition on Q_B binding site by specified compounds. The experimental methods concerning the fabrication of PS II-based biosensor and the electrochemistry measurement will be described in the following chapter. The results of detecting explosive/herbicide compounds will be presented in Chapter 4, where the performance of the biosensor and the mechanism of inhibition will also be studied.

We also attempted molecular modeling with a latest version of AutoDock program to simulate the conformation of explosive/herbicide binding to the Q_B pocket. These modeling studies are discussed in Chapter 5.

Chapter 2

Photosystem II

2.1 Basic principles of photosynthesis

Photosynthesis uses light energy to convert CO_2 into readily usable carbohydrates with water acting as the source of electrons and protons and O_2 forming as by-product. This process occurs in plants, algae and many species of bacteria. Essentially all life on Earth depends on photosynthesis, because it simultaneously generates an aerobic atmosphere, and provides energy either directly or indirectly to all organisms.

Chlorophyll was identified as the major light absorber for driving the process in 1874 [28]. Robert Emerson and William Arnold [29] demonstrated that several hundred Chl molecules worked together to produce one O_2 molecule. This led to the concept of the 'photosynthetic unit' as a network operating in O_2 evolving organisms, which is known as the photosystem nowadays.

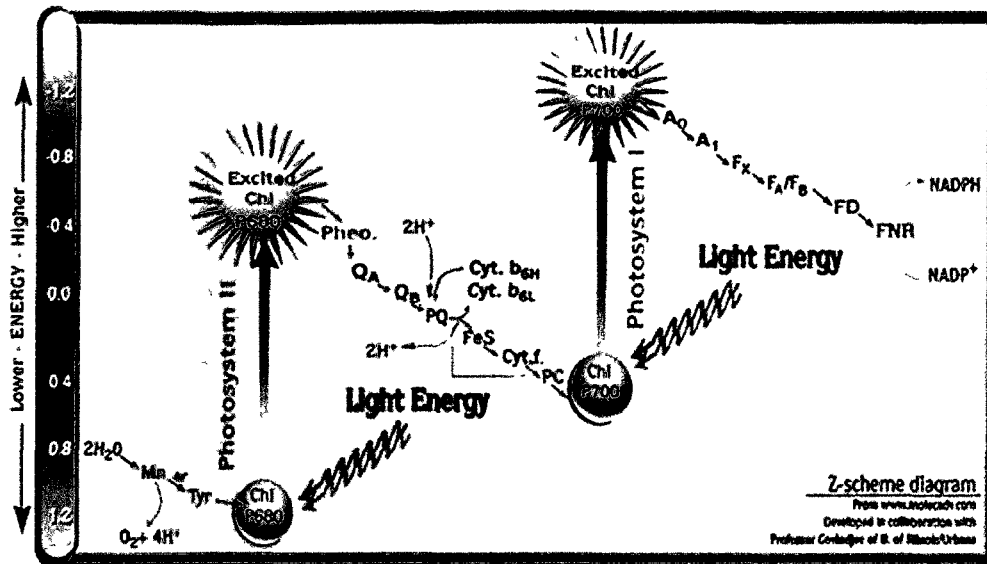


Figure 2.1.1: The Z-scheme of oxygenic photosynthesis

The Z-scheme of oxygenic photosynthesis for electron transfer from water to nicotinamide adenine dinucleotide phosphate (NADP) modified from Fig. 4 of Govindjee [30]. From left to right: Mn stands for Mn cluster; Tyr, for tyrosine-161 on the D1 protein; P680, for the primary electron donor of PS II; Pheo, for pheophytin; Q_A, for the first PQ electron acceptor of PS II; Q_B, for the second PQ electron acceptor of PS II; PQ, for the plastoquinone pool; Cyt b₆L and Cyt b₆H, for low and high potential cytochrome b₆; Cyt f, for cytochrome f; FeS, for Rieske iron sulfur; PC, for plastocyanin; P700, for the primary electron donor for PS I; A₀, for a monomer Chl; A₁, for vitamin K; F_x, F_A and F_B, for iron sulfur centers 'x', 'A' and 'B,' respectively; and FD, for ferredoxin.

The terms 'Photosystem I' and 'Photosystem II' were first proposed by Duysens [31] in his research of 'Z-scheme' (Figure 2.1.1) of oxygenic photosynthesis. In this scheme, PS II is shown as the functional unit transferring electrons from water to the plastoquinone (PQ), an electron acceptor that in turn donates electrons via the cytochrome (Cyt) complex to PS I, in which the NADP⁺ (Nicotinamide adenine dinucleotide phosphate) is reduced to NADPH. The whole electron transport generates a proton gradient across the thylakoid membrane. This proton motive force

is then used to drive the synthesis of ATP. Hence the role of PS II in the total process is a water/plastoquinone oxido-reductase (Figure 2.1.2).

In bacterial photosynthesis, BRC is responsible for transferring the electron to establish a proton gradient across the membrane, which is ultimately used by ATP synthetase to form ATP. The structure and function of the PS II are evolutionarily related to BRC, but are more complex and evolved. The homologies between BRC and PS II have been the foundation of the modeling for the PS II reaction center complex until structures of PS II from several organisms became available recently [32].

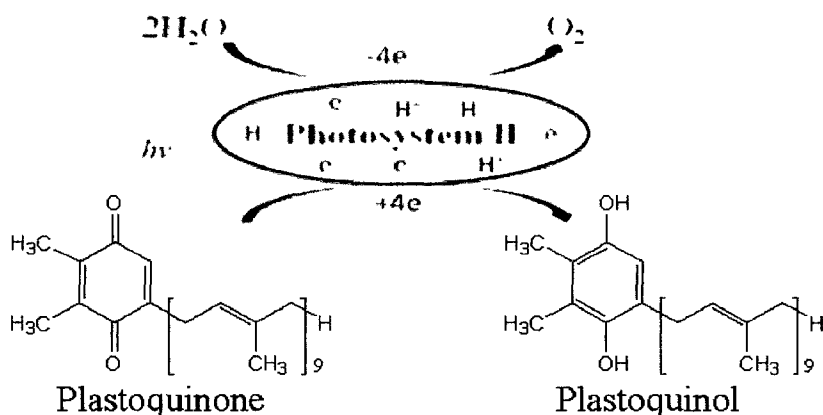


Figure 2.1.2: The overall reaction of PS II

The PS II reaction center uses light energy to oxidize water and to reduce plastoquinone.

2.2 Structure of PS II complex

PS II is located in the thylakoid membrane of plants, algae and cyanobacteria. The PS II complex spans the thylakoid membrane, with an oxygen evolving (water-splitting) center on the luminal side, a plastoquinone reduction site on the stromal side, and the light-harvesting chlorophyll antenna proteins (Figure 2.2.1 [33]). Over 20 subunits associating with other cofactors and light harvesting proteins are involved in the PS II complex. These components are named after the genes encoding them. The structure, cofactor organization, and function of these subunits have been studied in detail and are summarized in Table 2.2.1 [34].

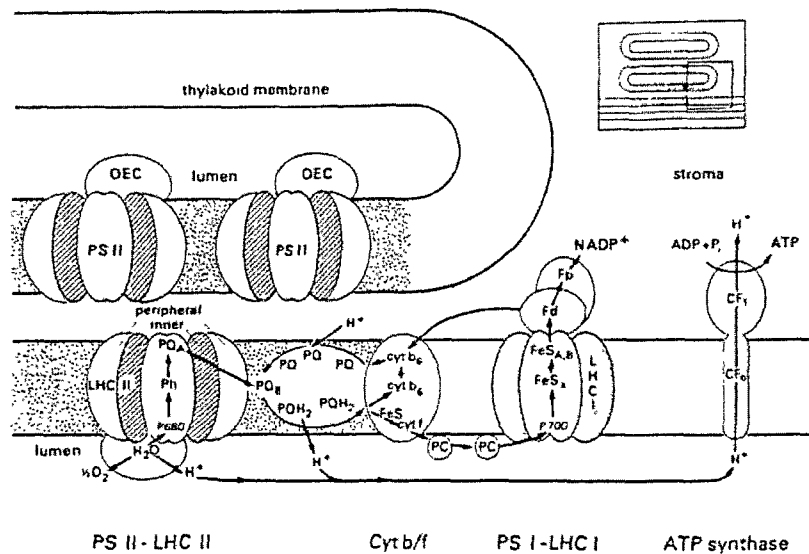


Figure 2.2.1: Organization of protein complexes in thylakoid membranes

LHC II and LHC I are peripheral light-harvesting chlorophyll proteins of PS II and PS I, respectively. OEC is oxygen-evolving complex.

Table 2.2.1: The PS II subunits: primary and secondary structure, and function

Gene	Subunit	Mass (kDa)	No. of α -helices	Function
<i>psbA</i>	D1	38.021	5	Yz & binds P680, Pheo, Q _B
<i>psbD</i>	D2	39.418	5	Yd & binds P680, Q _A
<i>psbE</i>	α -cyt b559	9.255	1	Binds heme, photoprotection
<i>psbF</i>	β -cyt b559	4.409	1	Binds heme, photoprotection
<i>psbI</i>	I protein	4.195	1	<i>Unknown</i>
<i>psbB</i>	CP47	56.278	6	Excitation energy transfer, binds 33 kDa
<i>psbC</i>	CP43	50.066	6	Excitation energy transfer binds 33 kDa
<i>psbH</i>	H protein	7.697	1	Photoprotection
<i>psbK</i>	K protein	4.283	1	PSII assembly, PSII stability
<i>psbL</i>	L protein	4.366	1	Involved in Q _A function
<i>psbM</i>	M protein	3.755	1	<i>Unknown</i>
<i>psbN</i>	N protein	4.722	1	<i>Unknown</i>
<i>psbO</i>	33-kDa ext. protein	26.539	0	Stabilizes Mn cluster,

Continued on next page

Table 2.2.1(continued)

Gene	Subunit	Mass (kDa)	No. of α -helices	Function
<i>psbP</i>	23-kDa ext. protein	20.21	0	Ca ²⁺ & Cl ⁻ binding Ca ²⁺ & Cl ⁻ binding
<i>psbQ</i>	16-kDa ext. protein	16.523	0	Ca ²⁺ & Cl ⁻ binding
<i>psbR</i>	R protein	10.236	0	Donor and acceptor side functions
<i>psbS</i>	S protein	21.705	4	Chl chaperonin/antenna component
<i>psbT</i>	T protein	3.283	0	<i>Unknown</i>
<i>psbV</i>	V protein	15.121	0	Donor side stability
<i>psbW</i>	W protein	5.928	1	<i>Unknown</i>
<i>psbX</i>	X protein	4.225	1	Q _A function
<i>lhcb4</i>	CP29	29	3	Excitation energy transfer & dissipation
<i>lhcb5</i>	CP26	26	3	Excitation energy transfer & dissipation
<i>lhcb6</i>	CP24	24	3	Excitation energy transfer

Continued on next page

Table 2.2.1(continued)

Gene	Subunit	Mass (kDa)	No. of α -helices	Function
				& dissipation
<i>psbJ</i>	J protein	4.116	1	PSII assembly
<i>psbU</i>	U protein	10	<i>Unknown</i>	<i>Unknown</i>
<i>lhcb1</i>	Lhcb1	25	3	Light harvesting
<i>lhcb2</i>	Lhcb2	25	3	Light harvesting
<i>lhcb3</i>	Lhcb3	25	3	Light harvesting

The core of PS II complex is composed of two subunits—D1 and D2. These two subunits are almost identical and are highly hydrophobic. They contain P680, the OEC, two pheophytins, two plastoquinones, and a non-heme iron ion. The overall structure of PS II is shown in Figure 2.2.2 [32]. D1 and D2 subunits each comprise five transmembrane helices organized in a manner almost identical to that of the L and M subunits of the BRC. Nevertheless, the C-terminal domains and the loops joining the transmembrane helices are more extended in the case of the D1 and D2 subunits compared with BRC, especially on the luminal side close to the OEC.

P680 stands for the pigments that play the key role in primary charge separation and are absorbing light at wavelength of 680 nm. It is a chlorophyll *a* multimer with outstanding features. Its cationic radical P680⁺ has one of the highest redox potentials found in nature, estimated to be 1.3 to 1.4 V, and is thereby capable of oxidating water through the OEC. On the basis of an X-ray study [32], OEC is a cubane-like Mn₃CaO₄ cluster linked to a fourth Mn ion by a mono- μ -oxo bridge. Specifically, each metal ion in this cluster has three- μ -oxo bridges (the large domain) connected to another Mn ion by a mono- μ -oxo bridge in the extended region. Q_A, non-heme Fe and Q_B are localized to face the matrix space of the chloroplast. The binding sites of Q_A and Q_B will be discussed later. The non-heme Fe is linked in between the two plastoquinones by histidine ligand bonds and mediates the electron transport from Q_A to Q_B. Two pheophytins, Pheo_{D1} and Pheo_{D2} are bound to D1 and D2, respectively. They are involved in the primary electron transfer in association with other reaction center pigments.

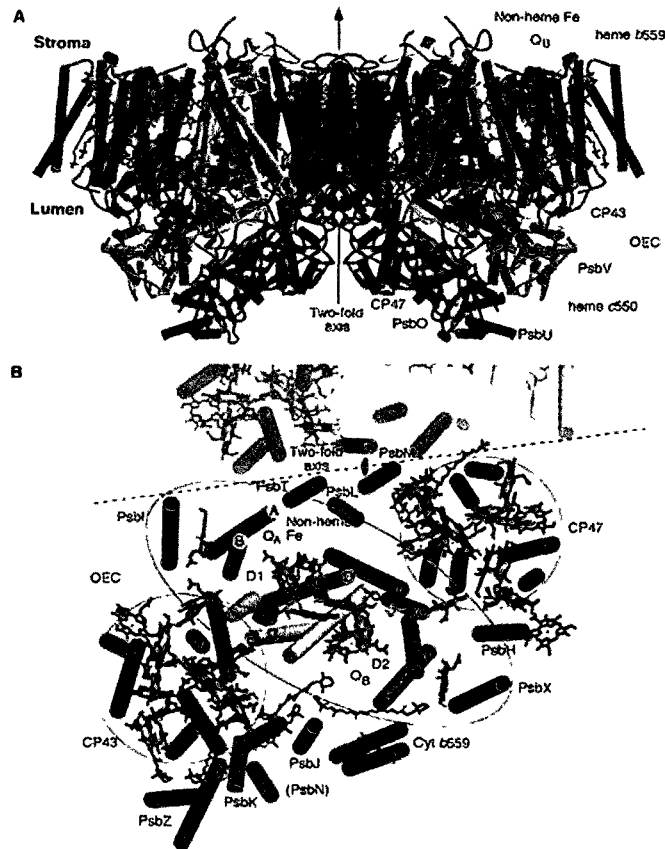


Figure 2.2.2: Overall Structure of PS II core complex

(A) View of the PSII dimer perpendicular to the membrane normal. Helices are represented as cylinders with D1 in yellow; D2 in orange; CP47 in red; CP43 in green; *cyt b559* in wine red; PsbL, PsbM, and PsbT in medium blue; and PsbH, PsbI, PsbJ, PsbK, PsbX, PsbZ, and the putative PsbN in gray. The extrinsic proteins are PsbO in blue, PsbU in magenta, and PsbV in cyan. Chlorophylls of the D1/D2 reaction center are light green, pheophytins are blue, chlorophylls of the antenna complexes are dark green, -carotenes are in orange, hemes are in red, non-heme Fe is red, Q_A and Q_B are purple. The OEC is shown as the red (oxygen atoms), magenta (Mn ions), and cyan (Ca²⁺) balls. (B) View of the PSII monomer along the membrane normal from the luminal side. A part of the other monomer in the dimer is shown to emphasize the region of monomer/monomer interaction along the dotted line. The pseudo-twofold axis perpendicular to the membrane plane passing through the non-heme Fe relates the transmembrane helices of the D1/D2 heterodimer, the low molecular subunits, PsbI and PsbX, and CP43 and CP47 as emphasized by the black lines encircling these subunits. Coloring is the same as in (A).

Flanking the opposite sides of the D1/D2 heterodimer are the CP43 and CP47 subunits which together carry about 30 core ‘antenna chlorophylls’ and transfer excitation energy to P680. Each antenna complex possesses six transmembrane helices that are arranged in pairs to form a trimer of dimers. The two antenna complexes and the RC heterodimer function together as a pseudo-symmetric CP43/D1-D2/CP47 core complex. The main function of CP43 and CP47 in energy transfer is to provide a conduit for excitation energy transfer from the exterior antennae (LHC) of the photosystem (the intrinsic LHC in green algae and higher plants, and the extrinsic phycobilosomes in most cyanobacteria and red algae) to the reaction center core. In addition to their roles as proximal antennae proteins for the photosystem, both CP47 and CP43 appear to interact with proteins associated with the site of water oxidation [35].

Among the other 10 subunits attached outside the core complex, Cyt *b559* is the largest and the only one whose function is known well. The other low molecular weight subunits are possibly involved in PS II assembly, stabilization, dimerization, and photo-protection [36]. Cyt *b559* is a heterodimer composed of one α -subunit (PsbE), one β -subunit, and a heme cofactor. It is unlikely to be involved in the primary electron transfer in PS II due to its very slow photo-oxidation and photo-reduction kinetics. Instead, it could participate in the secondary electron transfer that helps protect PS II from photodamage. Cyt *b559* is essential for PS II assembly [37].

2.3 Isolation of PS II

In the studies of photosynthesis, the isolation of minimum functional protein units is usually the first step. A remarkable achievement in this field was made by Boardman and Anderson [38] who were able to separate digitonin-solubilized spinach chloroplasts into two fractions that were each enriched in one of the two Photosystems, i.e., PS I and PS II. Based on the difference of molecular weight, these two fractions can be separated by centrifugation. PS II activity is associated with the membrane fraction enriched in Chl *b*, which is now known to contain the granum of thylakoid membranes (Figure 2.3.1). The concentration ratio of Chl *a* to Chl *b* should be between 2.9 and 3.2 in a successful isolation of PS II complex [39]. Figure 2.3.2 is the sucrose gradient showing different chlorophyll containing bands separated from the solubilized thylakoid membranes after centrifugation. PS II fraction is the bottom band in the figure.

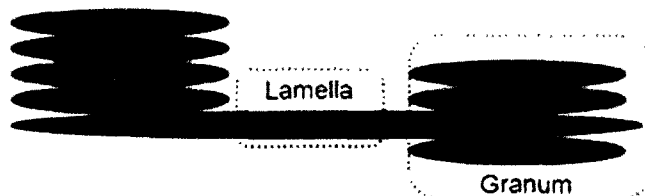


Figure 2.3.1: Thylakoid structures
Granum membranes of the thylakoid structures are enriched in PS II.

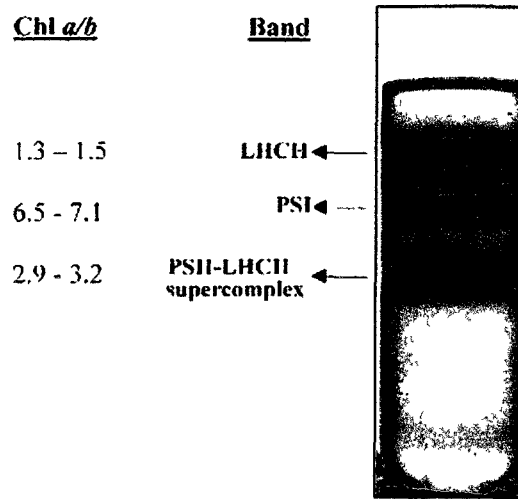


Figure 2.3.2: Different chlorophyll containing bands in different components of thylakoid membrane

During the early 1980s, a variety of methods using non-ionic detergents, e.g., sugar based detergents, were found to be effective in isolating protein complexes with PS II activity from a diverse range of cyanobacteria, green algae and higher plants [40]. The isolated PS II core complex consists of several major components, i.e., CP47 and CP43, D1 and D2 subunits, and Cyt *b559*. In addition to the major subunits, some other components such as *psbO* should be preserved to produce O₂. Refined preparations of this membrane fraction, e.g., the so-called BBY particles, retain full O₂-evolving activity and have been used extensively in the analysis of PS II structure and function. The name BBY was originated from Berthold, Babcock and Yocum who first developed the preparation method [41]. Non-ionic detergent Triton X-100 was used to separate the grana-stacked from the stroma-exposed region of the thylakoids.

2.4 Electron transfer process in the PS II complex

PS II complexes performing the electron transfer are located in the thylakoid membranes. Thylakoid membranes are either stacked (referred to as appressed or grana lamellae) or unstacked (referred to as stroma lamellae), and contain four membrane-spanning protein complexes involved in charge transfer: the PS II complex, the cytochrome complex, the PS I complex, and the ATP synthase complex. The electron transfer reactions in PS II are schemed in Figure 2.4.1 [42].

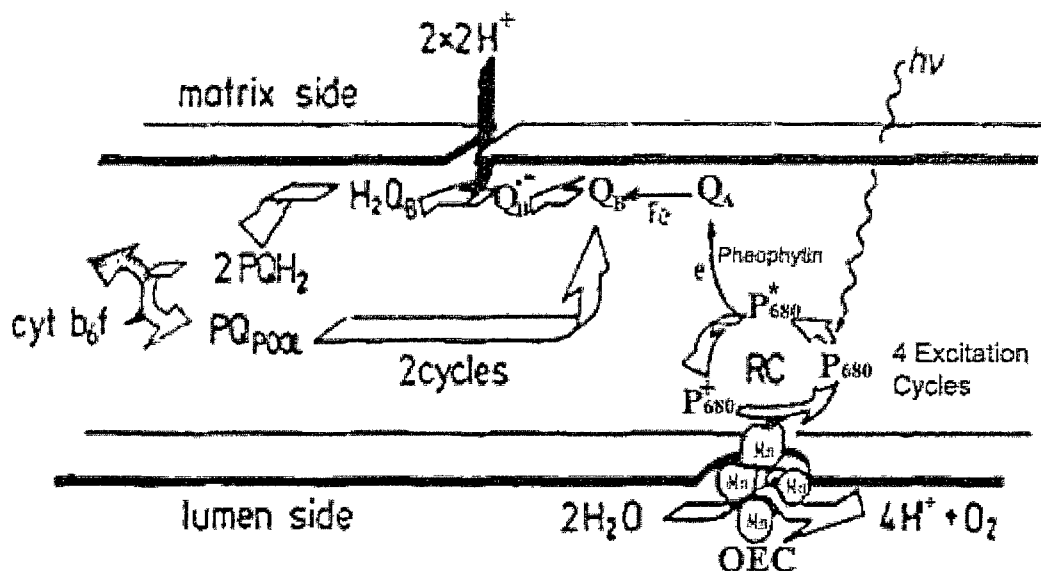


Figure 2.4.1: PS II primary electron transport and oxygen evolution

The reaction center P680 of PS II reduces Q_B via pheophytin and Q_A . Two excitation cycles are needed to reduce Q_B to the plastoquinol. Protons are taken up from the matrix space. The plastoquinol leaves the binding site on PS II and equilibrates with a larger plastoquinone/plastoquinol pool. Four excitation cycles through P680 are needed to oxidize the Mn_4CaO_3 complex. The fully oxidized manganese complex oxidizes 2 molecules of water to evolve one O_2 .

The primary electron transfer reactions in PS II consist of the initial charge separation and subsequent reduction of the primary donor by extracting electrons from water. Upon illumination, an electron is ejected from the excited primary electron donor P680, and in 10 picoseconds the electron is passed to the primary electron acceptor, Pheophytin Pheo_{D1}. Once the primary charge separation takes place, the secondary electron transfer in PS II rapidly stabilizes the electron flow to reduce a back reaction. After the first charge separation step the oxidized P680 is reduced to its initial state by the OEC. Four consecutive oxidation steps in the OEC produce one oxygen molecule from water. The pheophytin in turn reduces the first plastoquinone in the electron transfer system (Q_A) in about one nanosecond. Q_A is reduced only to the semiquinone state (PQH), which remains bound tightly to the D2 subunit. This radical anion semiquinone reduces the final electron acceptor, Q_B , which is bound loosely to the D1 subunit. After a second similar light-driven excitation cycle, Q_B accepts a second electron and becomes reduced to plastoquinol (PQH₂). The protonated plastoquinone leaves the quinone binding site and is replaced by another molecule from the plastoquinone pool within the membrane and afterwards the overall reaction cycle continues. The protonated plastoquinone can move freely either in the membrane or across it. It thus becomes the first electron donor in the PS I electron transport system. Upon illumination the PS I reduces NADP⁺ using the electron transferred via the plastocyanin Cyt *b₆f*.

In the first step of the primary electron transfer, the generated P680⁺ is a long-lived strong oxidant that can potentially damage the protein unless it is reduced. If

reduction of $P680^+$ is blocked, then secondary electron transfer occurs that ultimately results in the oxidation of Cyt *b559* [43]. It has also been found that Cyt *b559* can be reduced by electrons generated within PS II. Buser et al. [44] found that doubly reduced quinone PQH_2 can reduce Cyt *b559*. Therefore the overall role of Cyt *b559* in the PS II electron transfer is to act as an emergency electron donor or acceptor [45, 46].

The protons split from water are released into the inner lumen side of the thylakoid membrane, whereas the protons needed to reduce plastoquinone are taken from the matrix space. As a result a proton concentration gradient is established between the inner and outer space of the thylakoid membrane, a consequence of vectorial electron flow across the membrane.

2.5 Quinone binding site in PS II

The architecture of the polypeptides involved in Q_A , Fe and Q_B binding in PS II is quite analogous to that of the bacterial system (Figure 2.5.1 [32]). Even though PS II and BRCs use different quinone acceptors, the model of PS II based on the study on BRCs proved very successful. The overall view of the iron-quinone complex is shown in Figure 2.5.2 [32]. The binding sites for Q_A and Q_B are localized in D2 and D1 subunit, respectively. Helices IV and V of each subunit are of particular relevance of quinone binding. The non-heme Fe, which mediates electron transfer from Q_A to Q_B , is positioned on a pseudo-twofold axis of the D1/D2 heterodimer.

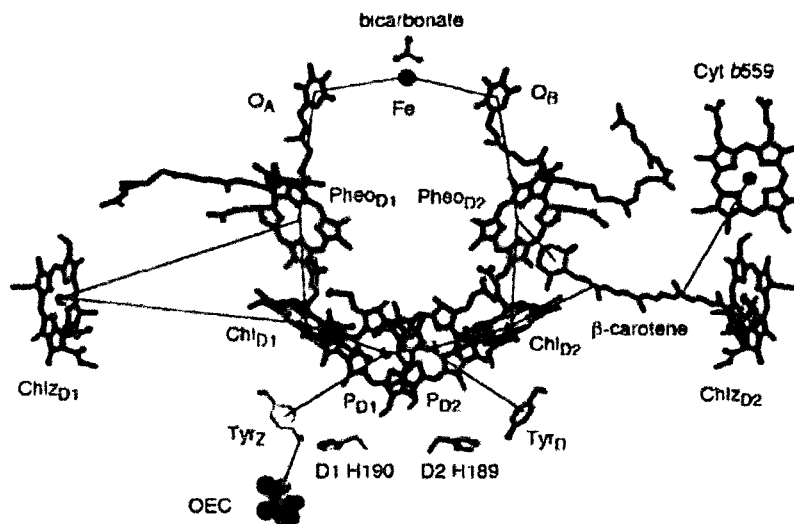


Figure 2.5.1: PS II RC cofactors involved in electron transfer

Electron transfer cofactors shown perpendicular to the internal pseudo-twofold axis. Coloring scheme is the same as in Figure 2.2.2. The phytol tails of the chlorophylls and pheophytins have been removed for clarity. The side chains of Tyr_Z (D1 Tyr161) and D1 His190 are shown in yellow, and Tyr_D (D2 Tyr160) and D2 His189 are in orange. The four chlorophylls comprising P680 are in direct van der Waals contact, and other electron transfer distances are given in Å.

X-ray study [36] proposed that Q_A is firmly bound to the main-chain amide group of Phe261 and His214 on the D2 subunit, where the latter also serves as a ligand to the Fe ion (Figure 2.5.2, A and B). The Q_A pocket is a hydrophobic cavity composed of multiple residues on D2 subunit including Ile213, Thr217, Met246, Ala249, Trp253, Ala260, and Leu267.

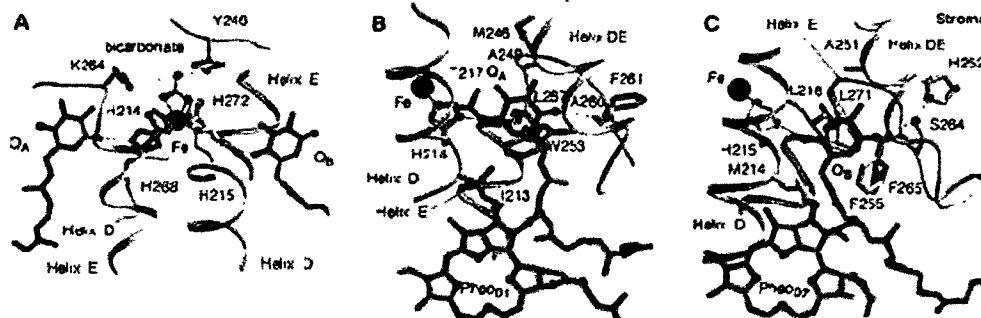


Figure 2.5.2: Electron acceptors of PS II

(A) Overall view of the nonheme iron, Q_A and Q_B . Coloring scheme is as in Figure 2.2.2, with protein main chains depicted in gray and with side-chain bonds and carbon atoms following the coloring of the protein subunit as used in Figure 2.2.2. The bicarbonate that completes the coordination sphere of the nonheme Fe is shown as magenta balls and is probably hydrogen bonded to D2 Lys264 and D1 Tyr246. (B) The Q_A binding pocket. The hydrophobic residues forming this pocket are shown. The O_1 of the plastoquinone head group is likely to be hydrogen bonded to the nonheme Fe ligating D2 His214 by its δ -nitrogen, whereas the O_4 atom may hydrogen bond to the backbone amide nitrogen of D2 Phe261. (C) The Q_B binding pocket. Q_B binds deep into a cavity lined with the hydrophobic residues. O_1 is likely to be hydrogen bonded to the δ -nitrogen of D1 His215, which also forms a ligand to the nonheme Fe, whereas O_4 may form hydrogen bonds with the amide nitrogen of D1 Phe265 and the side chain γ -oxygen of D1 Ser264. D1 Ser264 appears to make further hydrogen-bonding contact with D1 His252. Probable hydrogen bonds are shown as dotted lines; solid lines represent ligands.

There are four histidines (D1 His215, D1 His272, D2 His214, and D2 His268) responsible for the nonheme Fe binding. It has also been suggested that bicarbonate may serve as the fifth ligand to the nonheme Fe in PS II and that it has a regulatory function involving electron flow from Q_A to Q_B as well as facilitating the reduction of Q_B [32].

The plastoquinone in the Q_B site is hydrogen bonded to D1 Ser264 and D1 His215, where the latter one is also a ligand for the nonheme Fe. It is also possible that Q_B is bonded to D1 Phe265 on the main-chain. The Q_B pocket is comprised of D1 residues Met214, Leu218, Ala251, Phe255 and Leu271 (Figure 2.5.2, C). In addition, because D1 His252 is within hydrogen-bonding distance of D1 Ser264, this residue could aid the protonation of Q_B [8]. Protonatable groups close to the quinone make the Q_B site more hydrophilic than the Q_A site. This property is essential to the conversion of quinone to PQH_2 , because the protonation reactions require an aqueous phase.

2.6 Binding of the inhibitors at the Q_B site

In the primary electron transfer process, Q_A and Q_B associate with non-heme Fe to perform as a two electron gate system. The kinetics of electron transfer involving the two electron gate has been studied through use of a fluorescence spectroscopy method [47]. It was suggested that the Q_B binding constant is relatively small, and a rapid movement of the quinone in and out of the site occurs. This dynamic association is required for the quinone to act to couple electron and proton transfer, and it provides the possibility of inhibition of the transiently unoccupied site by a quinone analogue. On the other hand, because of the inaccessibility and the lack of exchangeability of the plastoquinone when bound, the Q_A site is not a good target for inhibitors.

The plastoquinone in the Q_B site is reduced in two steps, therefore the Q_B site is supposed to bind nonreduced as well as singly reduced plastoquinone. This dual and

undemanding binding property of the Q_B site makes it possible to replace quinone by diversity of other chemicals. Many photosynthesis inhibitors, such as some herbicides bind to the Q_B site on the D1 subunit. It has been well established that treatment of plants with some herbicides blocks PS II electron transport, and thus also blocks the transfer of excitation energy from chlorophyll molecules to the PS II reaction center [33].

Three chemical families, the nitrophenols, nitriles, and pyridazinones, inhibit photosynthesis by preventing Q_B binding. The inhibitors bind to the Q_B site due to hydrogen bonds, van der Waals forces, and hydrophobic interactions depending on the chemical structures and properties of the inhibitors.

The binding schemes of plastoquinone and atrazine on the Q_B site are shown in Figure 2.6.1. The protein structure in the scheme is based on the BRC model. Hydrogen bonds between atrazine and the amino acids Ser264 and Phe265 are essential for atrazine binding. Phe255 contributes to hydrophobic interactions in herbicide binding [33]. This competitive binding blocks the access of quinone molecules to the Q_B site. Because atrazine cannot uptake proton and electron under this condition, the electron transport via Q_B site is disrupted. Trebst [48] proposed that herbicides of the nitrophenol and nitrile families probably bind to the Q_B site due to the interactions with His215 rather than Ser264.

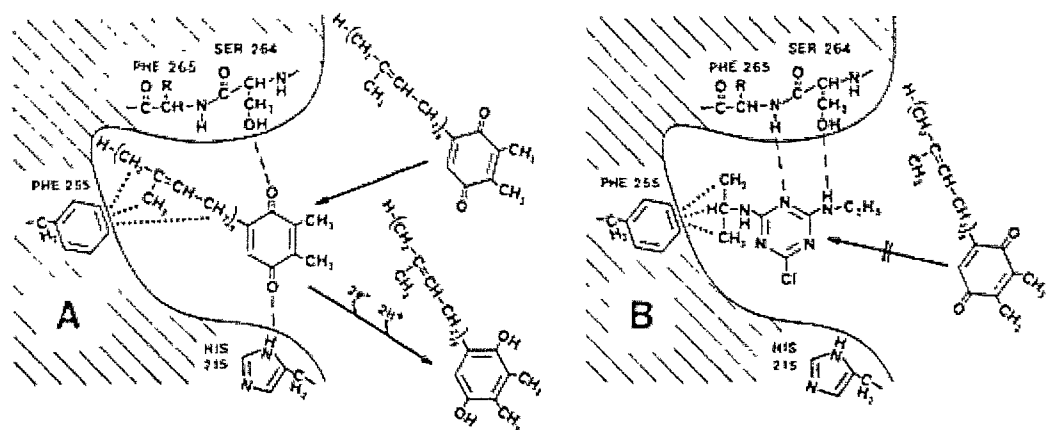


Figure 2.6.1: Schematic figure of the plastoquinone/herbicide binding pocket of the D1 protein

Dashed lines represent hydrogen bonds; dotted lines represent hydrophobic interactions. (A) Plastoquinone binds to the D1 protein, accepts two electrons and two protons, and is released as plastohydroquinone. (B) Atrazine binds to the D1 protein and prevents the binding of plastoquinone [33].

Upon illumination, Q_A is reduced to form a $Q_A^-Q_B$ state which in turn can evolve into $Q_A^-Q_B^-$. However, if the Q_B site is vacant or occupied by the inhibitor the last step cannot occur and the electron transfer is disrupted as depicted in Figure 2.6.2 [47].

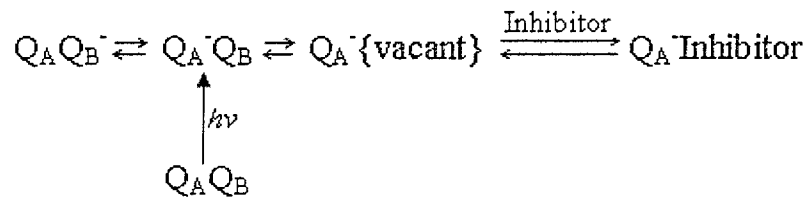


Figure 2.6.2: Displacement of Q_B by inhibitors

Summarizing, the PS II inhibitors interfere with Q_B function and thus block PS II electron transport activity in a concentration-dependent manner. Additionally, some classes of the inhibitors have other modes of action on photosynthetic organisms, not involving the Q_B site. For instance, nitrophenols also act on respiratory phosphorylation as an uncoupling inhibitor [42]. This property enhances their inhibitory potency. Nitric oxide, cyanide and carboxylate anions are found to be capable of binding reversibly at the non-heme iron site in competition with bicarbonate, resulting in most cases in deceleration of the electron transfer.

Advances in the understanding of inhibitory mechanisms naturally gave strong impetus to detection of herbicide research as well. The PS II-based biosensor for detection of herbicides [10, 9] has been well developed in the past decade. Photosynthetic assays can be done in a cell-free system, that is, with isolated thylakoid membranes, to obtain a direct measurement of its interaction with the inhibitors without the secondary effects from other components of intact plant tissues. The inhibitory potency of a herbicide can be evaluated via measuring the inhibitor concentration at which the photosynthetic activity is reduced by half [49].

Based on the structural similarity between nitric explosives and herbicides (Figure 2.6.3), it is suggested that some nitric explosives may also cause inhibitory effect on different plant species [50, 51]. Ali et al. [23] observed the inhibition of photosynthetic electron transport caused by TNT which can be evaluated via the decrease of chlorophyll *a* variable fluorescence field. However, it has not been proven that it is the inhibition of PS II involving the Q_B site and not some other effect which caused

this fluorescence decrease. In this work we are exploring the possibility that at least some nitric explosives work on PS II, especially on the Q_B site. The electrochemistry method will be applied for the detection of nitric explosives possibly involving Q_B site binding. The major objective of our research is to produce a sensitive PS II-based biosensor for detection of nitric explosives.

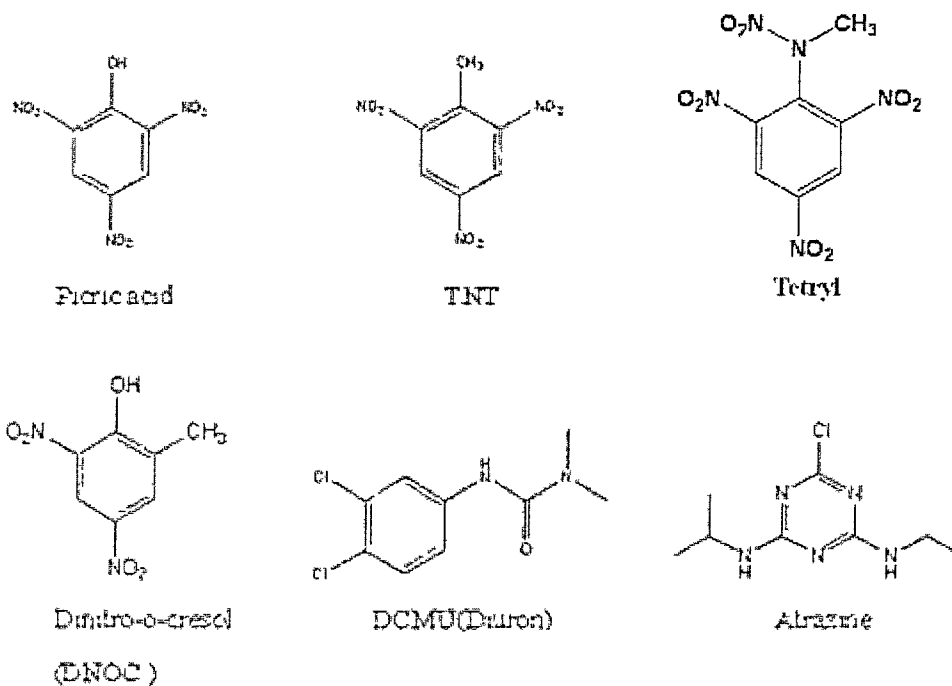


Figure 2.6.3: Herbicides as PS II inhibitors and explosives as potential inhibitors

Chapter 3

Material and Method

3.1 Preparation of PS II samples

The PS II samples were isolated from supermarket baby spinach leaves. Baby spinach leaves were kept in the dark at 4°C overnight before use to preserve the PS II activity as much as possible. All chemicals except TNT were ordered from Sigma-Aldrich. TNT was purchased from ChemServices, Inc. All preparations were carried out in a dark room with dim green light and at 4°C.

3.1.1 Purification of thylakoid membranes

Thylakoid membranes were prepared by treatment with sonication as described in CA patent 2412206 [52]. After washing with ice-cold water, deveined spinach leaves were crushed in a blender with a homogenizing buffer (Table 3.6.1). The mixture was cooled in an ice bath for 2 min after 1 min of crushing. The resulting slurry containing tissues and cells of spinach leaves was cooled again until the foam disappeared.

The homogenate was filtered through 16 layers of cheese cloth to remove impurities and the filtrate was centrifuged for 2 min at 2500 *g* at 4°C. The collected pellet was then resuspended in a 20 times diluted homogenizing buffer to a concentration of 2 mg Chl/mL and gently stirred for 30min. The resulting solution was lysed with 40 minutes of sonication in 1min intervals using a Mandel Scientific company's ultrasound processor in an ice bath to avoid excessive temperature. Purified thylakoid membrane was then collected after a centrifugation at 3500 *g*'s at 4°C for 3 min. The final pellet was stored at -80°C in the dark until use.

UV-Vis spectroscopic method was used to determine the concentration of chlorophyll in the suspension and the purity of isolated PS II [53]. In order to obtain a pure PS II sample, the A_{675}/A_{645} ratio should be between 2.9 and 3.2 [39, 54]. The spectrophotometric measurements were taken in quartz cuvette with a Cary 5000 UV-Vis with the following parameters:

Average time to scan: 0.033 s Data interval: 0.5 nm Scan rate: 909.091 nm/min
Spectral bandwidth: 2nm

The concentration of PS II complex in buffer is defined as the concentration of chlorophylls. The calculation of concentrations of pigments is as follows:

$$[\text{Chl } a] = (12.7 \times A_{675} - 2.69 \times A_{645})\mu\text{g/mL} \quad (3.1.1)$$

$$[\text{Chl } b] = (22.9 \times A_{645} - 4.68 \times A_{675})\mu\text{g/mL} \quad (3.1.2)$$

$$[\text{Total Chl}] = (8.02 \times A_{675} + 20.21 \times A_{645})\mu\text{g/mL} \quad (3.1.3)$$

where A_{675} and A_{645} are the absorbance at wavelengths 675 nm and 645 nm respectively.

3.1.2 Purification of BBY Membranes

BBY membranes were obtained using treatment with non-ionic detergent Triton X-100 as described by van Leeuwen et al. [54]. Triton X-100 is able to separate the granum stacks from the stroma-exposed regions of the thylakoids. More discussion on the function of Triton X-100 will be presented in Chapter 4.

The leaves were washed, depetiolated and then crushed with a blender in an isolation buffer following the same steps as described in subsection 3.1.1. After a filtration the suspension was centrifuged at 10,000 g 's at 4°C for 10 minutes. Pellets were collected and resuspended in the isolation buffer to a concentration of 2 mg Chl/ml. With a gentle stirring, Triton X-100 solution was added to the suspension to a final concentration of 25 mg/mg Chl. This ratio was chosen for the high efficiency of separation and the maximal conservation of OEC. Low concentration of the detergent causes incomplete separation of PS II particles. However, overexposure to the detergent may also remove OEC from the particle and damage the oxygen activity. The solubilization process lasted with stirring in the ice bath for about 15 min until the cells were lysed and PS II particles were concentrated through hydrophobic reactions with the detergent. The other proteins and components in thylakoid membranes are solubilized in the buffer. At this step the incubated suspension included soluble proteins, PS II particles surrounded by hydrophobic detergent molecules, and starch,

which is the component with the largest density. The PS II particles were isolated from the suspension by 3 steps of centrifugations. After the first centrifugation at 40,000 *g*'s at 4°C for 25 minutes, the PS II particles containing starch were collected and resuspended in the isolation buffer supplemented with 0.4 *M* sucrose, then centrifuged for 5 min at 2,000 *g*'s to remove starch. The supernatant containing the purified membranes was then sedimented once more for 25 min at 40,000 *g*'s. The purified BBY membranes in the sediment can then be stored at 80°C over periods as long as six months until use [55].

3.2 DCPIP assay

DCPIP is a chemical compound used as a redox-sensitive dye. Oxidized DCPIP is blue, reduced form is colorless. DCPIP assay is a conventional method in the study of rate of photosynthesis. As DCPIP is reduced and becomes colorless, and the resulting decrease in absorbance at around 600 nm can be measured by a spectrophotometer. All the procedures of DCPIP assay were carried out in dark except when illumination was needed.

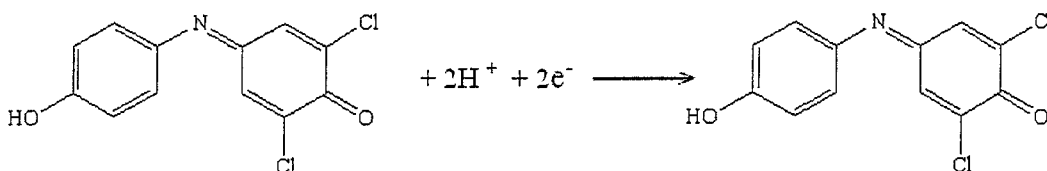


Figure 3.2.1: The reduction of DCPIP

3.2.1 Photosynthetic activity

The photosynthetic activities of the isolated PS II samples were determined by a DCPIP assay. With illumination, the photoreduction rate of the PS II sample in the presence of DCPIP was measured with Cary 5000 UV-Vis spectrophotometer. The spectrophotometric parameters were the same as described in section 3.1.1. Unfrozen PS II samples were resuspended in a pH 7.5 measuring buffer to a concentration of 2mg Chl/mL. Vortex was used to help disperse the PS II particles. The resulting PS II solution was taken for the baseline. In the measurement, the photoreduction occurred in a solution which contained 20 μg Chl/mL of PS II particles and 0.15mM of DCPIP. The sample was then illuminated with a halogen lamp light from one side for 10 seconds. The intensity of the light was $1.5 \times 10^4 \text{ W/m}^2$. This step was repeated until the absorbance was below 0.2. The decrease of the absorbance at $\sim 590 \text{ nm}$ upon illumination is proportional to the rate of the photoreduction of DCPIP catalyzed by PS II complex, so that the photosynthetic activity can be calculated as the rate of photoreduction as follows:

$$\text{Photosynthetic activity} = \frac{\Delta A_{\text{DCPIP}}}{e \times l \times V \times m_{\text{PS II}} \times t} \quad (3.2.1)$$

here, ΔA_{DCPIP} is the decreased peak absorbance of DCPIP after illumination; e is extinction coefficient of DCPIP ($2.1 \times 10^4 \text{ M}^{-1} \text{ cm}^{-1}$), l is the width of the cuvette (1cm); V is the volume of the solution; $m_{\text{PS II}}$ is the mass of the chlorophyll in the PS II particles used in the measurement and t is illumination time.

3.2.2 Effect of PS II inhibitors on DCPIP measurement

To study the effect of herbicides and explosives on photosynthetic activity, the rate of photoreduction of DCPIP was measured in the presence of explosive molecules. Explosives were added to the DCPIP-PS II suspension to obtain a series of increasing concentrations. Each time the absorbance was measured with an illumination of 10 seconds. And the spectrum of PS II suspension was taken for the baseline during each concentration-dependant measurement respectively. The presence of explosives affects the photoreduction of DCPIP in the manner of inhibiting PS II activity. In this case, the residual activity of PS II equals to the ratio of the photoreduction rate in the presence of explosive to that in the absence of explosive which can be calculated as follows,

$$\text{Residual Activity}(\%) = \frac{\Delta A'_{\text{DCPIP}}(\text{in presence of inhibitor})}{\Delta A'_{\text{DCPIP}}(\text{in absence of inhibitor})} \times 100\% \quad (3.2.2)$$

The data were plotted as residual activity vs. concentration of explosive.

3.3 Immobilization of PS II particles for the biosensor

The DRP-220 gold screen printed electrodes were purchased from DropSens company. The electrode assembly consists of a gold working electrode with the area of 0.13 cm², a graphite counter electrode and an Ag/AgCl reference electrode. The immobilization

process should avoid damaging the activity of the PS II protein or affecting its activity as much as possible and therefore needs to be done in a quick and safe way.

The procedure of BSA-glutaraldehyde matrix based immobilization was similar to the one described by Loranger and Carpentier [56, 57]. PS II samples were first dissolved in a pH 6.5 measuring buffer to obtain a PS II suspension at the concentration of 2mg Chl/mL. A 10% solution of BSA in the measuring buffer was mixed with equal amount of PS II solution. For cross-linking purpose a 10% glutaraldehyde solution was added to a final concentration of 0.3%. The glutaraldehyde cross-links the -SH groups of cysteine residues to form a matrix on the surface of the electrodes. A droplet of 2.5 μ l of the mixture was spread over the working electrode for its selective functionalization and incubated for 30 min at 4°C in dark for the matrix formation without interference. The electrodes functionalized with PS II were stored at -20°C in the dark for at least 6 hours before use. The immobilization of the photosynthetic material is visible as a green deposition on the electrodes. The electrode is recyclable after washing off the PS II samples with ethanol and drying it with nitrogen.

3.4 Photo-electrochemical measurements

The measurements with the biosensor were carried out at room temperature in the dark except for the pulse illumination. The detection of electrochemical signals on the PS II-functionalized electrodes was performed using the CHI630C electrochemical

workstation from CH Instruments, USA. The light source was either a 670 nm 7 mW laser photodiode or, for measurements at different wavelengths, the Spectra-Physics / Sirah Matisse CW dye laser. The optimal illumination wavelength was determined by measuring the photocurrent signals of PS II-functionalized electrodes with a pulse illumination at different wavelengths. Electrochemical measurements were performed by placing a 50 μ l droplet of the electrolyte containing analyte onto the working area to cover the three electrodes.

DQ and FeCy were used as mediators with concentrations of 0.2mM and 1mM respectively. The redox potentials of the two mediators were determined by a cyclic-voltammetry method [58]. A triangular wave form of potential sweep was applied to a working electrode, and gave rise to a reversible current-potential (i-E) curve during the reversible electron transfer step on the working electrode. Figure 3.4.1 is the curve of a theoretical cyclic voltammogram. The anodic and cathodic peaks on the curve present the oxidation potential and reduction potential respectively. The location of redox potential of the mediator is the midpoint of the two peaks. The measurement parameters are as followed:

Potential scan rate: 1 mV/s

Potential scan range: -1.0 V to 1.0 V

Current sensitivity: 1 μ A

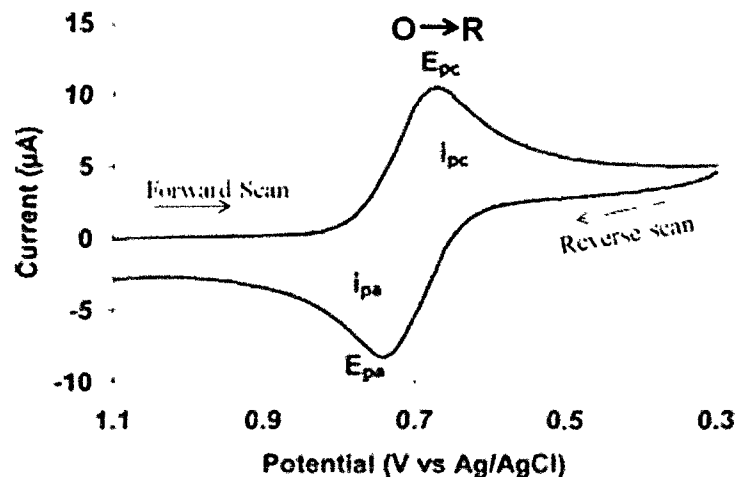


Figure 3.4.1: Theoretical cyclic voltammogram
 Theoretical cyclic voltammogram modified from figure in [59], where i_{pc} and i_{pa} show the peak cathodic and anodic current respectively for a reversible reaction.

In the measurement of photo-current, the working electrode of the biosensor was polarized at 0.62 V for DQ (0.2 mM) or 0.36 V for FeCy (1 mM).

In order to detect explosives (or herbicides) in the measuring buffer, a current-time (i-t) curve was measured while the sensor was illuminated with a light pulse. The signal detection was first optimized with the mediator in a pH 6.5 measuring buffer without PS II inhibitors to obtain a steady current baseline. The droplet was then carefully removed with the pipette and the biosensor was rinsed twice with measuring buffer before a new droplet was added. After the explosives were added to the pH 6.5 measuring buffer in the presence of mediator, the biosensor was incubated for 10 minutes in the dark until some diffusion took place and the photo-induced current was expected to become steady. The electrode with droplet was illuminated to obtain a current signal. Values of current peaks were measured to

calculate the relative activities. Upon the measurements of photo-induced current at different concentrations of analytes, a curve of relative activity versus concentration was obtained to characterize the inhibition mechanism.

In order to compare the inhibition mechanism of explosives to that of herbicides, the detection of herbicide was performed as well through the same procedure as described above.

The detection parameters are as followed:

Sensitivity: 1 nA

Potential with respect to reference electrode: 0.62 V for DQ (0.2 mM)

0.36 V for FeCy (1 mM)

Incubation time: 10 min

Illumination wavelength: 670 nm

Illumination intensity: 8 W/cm²

Illumination time: 5 s

In the detection of photosynthesis inhibitors, the current increases as a result of the light-induced redox reaction and the resulting peak current depends on the activity of PS II. As shown in Figure 3.4.2 the residual activity of PS II therefore equals to the ratio of the amplitude in the presence of inhibitors to that in the absence of inhibitors.

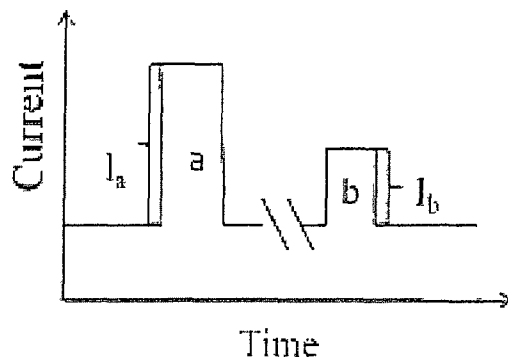


Figure 3.4.2: Scheme of amprometric readout upon increasing the concentration of the inhibitors.

Peak (a) is a light-induced signal in the absence of inhibitors; Peak (b) is a light-induced signal in the presence of inhibitors. Residual activity = $I_b/I_a \times 100\%$.

3.5 Analysis of inhibitor binding

The residual activities of PS II vary upon the concentrations of the inhibitors. The residual activity vs. concentration curves were fitted with logistics equation:

$$y = y_{min} + \frac{y_{max} - y_{min}}{1 + (x/EC50)^{Hill\ slope}} \quad (3.5.1)$$

where,

y_{max} : maximum residual activity

y_{min} : minimum residual activity

EC50: concentration of inhibitor which causes a 50 % inhibition of the activity

Hill slope: coefficient which describes the cooperativity of the binding.

The EC50 also represents the dissociation constant of the PS II-inhibitor binding.

The LOD was determined on the basis of 99 % confidence interval, which, assuming the normal distribution, corresponds to $2.6 \times$ standard error of the measurement (σ) [60]. Then the LOD was calculated as

$$LOD = \frac{2.6 \times \sigma \times EC50}{100 - 2.6 \times \sigma} \quad (3.5.2)$$

3.6 Components of buffers

The compositions of various buffers used in this study are presented in Table 3.6.1.

Table 3.6.1: Components of buffers

Buffer	Components
Homogenizing Buffer	20mM Tricine (pH 7.5), 330mM sorbitol, 5mM MgCl ₂
Isolation Buffer	20mM MES (pH 6.0), 15mM NaCl and 5mM CaCl ₂
pH 7.5 Measuring Buffer	20mM Tricine, 0.2mM sucrose, 10mM KCl, 3mM MgCl ₂
pH 6.5 Measuring Buffer	15mM MES, 0.5 M mannitol, 0.1 M NaCl, 5mM MgCl ₂ , $5 \times 10^{-5} M$ chloramphenicol

Chapter 4

Detection of explosives/herbicides with biosensor

4.1 Principle of detection using biosensor

The presence of explosive/herbicide in a solution is detected as a decrease of photocurrent signal in the presence of mediator compared to the activity in the absence of the explosive/herbicide. The photocurrent is generated through the redox reaction of the mediators in the solution, which indirectly represents the PS II activity upon illumination.

As discussed in section 2.4, when the light harvesting complexes transfer the excitation energy to the PS II reaction center, the PS II electron transport takes place. From pheophytin, the excited electron derived from the splitting of water is transferred to Q_A and then Q_B . Q_B accepts two electrons from Q_A and two protons from the stroma side of the thylakoid membrane, and then leaves its binding site as plastoquinol. In vivo, plastoquinol as the product of PS II electron transport donates

its electrons to the Cyt b_6f complex to connect the electron transport between PS II and PS I. The mediators such as FeCy and DQ in this study work as artificial electron acceptors instead of plastoquinone when reacting with the PS II reaction center. In the measurement, the working electrode is polarized at the corresponding redox potential of the mediator so that the reduced electron acceptor is re-oxidized and a current signal is observed. The mass transfer of the electrons thereby is proportional the PS II activity. The explosive or herbicide in the solution inhibits the access of mediator in to the Q_B pocket. The mediator cannot be reduced by plastoquinol and consequently no current is generated.

Figure 4.1.1 depicts an example of DCMU detection. The signals from left to right are due to an increasing concentration of DCMU in the pH 6.5 measuring buffer in the presence of DQ. The baseline corresponds the background current of the oxidized DQ in the dark. The first peak is the control signal in the absence of DCMU. Then, DCMU was loaded into the solution and the signal induced by the light pulse was recorded. The decrease of the signal magnitude indicates the reduction of PS II activity by DCMU. The ratio of the signals in the presence and absence of the herbicide was calculated.

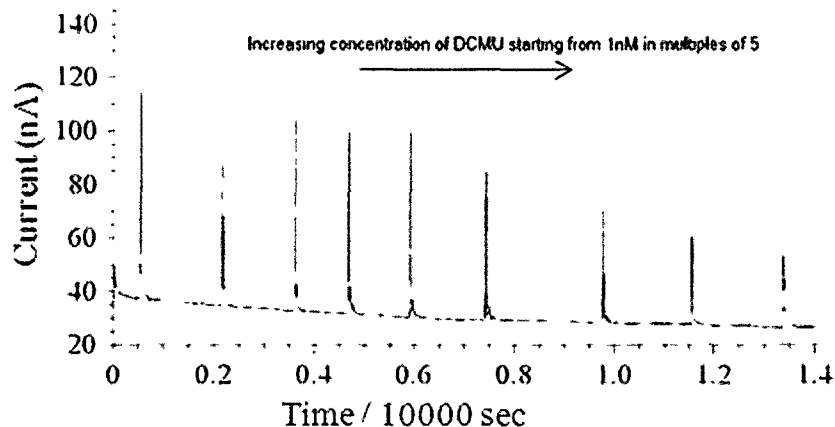


Figure 4.1.1: Photocurrent signals of DCMU detection
 The presence of DCMU was detected from a decrease of the photocurrent signal in the presence of DQ.

4.2 Characteristics of the PS II membranes

Stability and sensitivity, which are essentially related to the quality of the prepared PS II samples, are important parameters of a biosensor. In this section, factors such as the purity, the activity and the half life of the samples are considered.

The PS II-enriched membranes, i.e. the BBY membranes are thylakoid membranes solubilized with the non-ionic detergent Triton X-100. The function of Triton X-100 is to separate the lamella part from the intact thylakoid by hydrophobic reactions and consequently to concentrate the granum stacks (Figure 2.3.1) through hydrophobic reactions. The PS II complex is more concentrated in the stack structure of the thylakoid membrane, whereas the lamella contains more PS I. The

spectra of PS II preparations are shown in Figure 4.2.1. Each PS II particle sample collected after centrifugation was diluted 100 times with the buffer used in the preparation. The peak absorbance of Chl *a* has shifted to 675 nm and 436 nm, while the peak of Chl *b* has shifted to 645 nm and 471 nm.

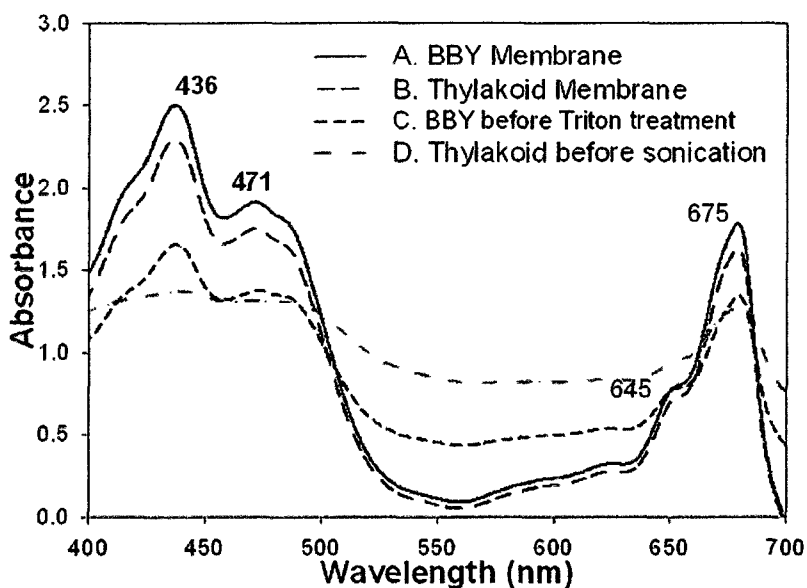


Figure 4.2.1: UV-Vis spectra of PS II particles during preparations

The chlorophyll content of each sample in Figure 4.2.1 is calculated (Table 4.2.1). By comparing the A_{675}/A_{645} values it is clear that Triton X-100 treatment is efficient in separating PS I and PS II. The oxygen activity of BBY membrane is therefore significantly higher than that of thylakoid membrane. Measured by spectroscopy, the BBY membranes has an oxygen activity of 100 to 300 $\mu\text{mol O}_2/\text{mg Chl/h}$, and

the thylakoid membrane has about $50 \mu\text{mol O}_2/\text{mg Chl}/\text{h}$. It has been reported that thylakoid membranes were used for BSA-matrix formation on the biosensor electrodes and a photocurrent signal stable for long time (half life of 16.7h in the presence of DQ) has been observed [61, 62]. On the other hand, the half life of PS II enriched membrane-based biosensor is 8h in the presence of DQ, according to Koblizek et al. [10, 9]. The half lives of both types of the biosensors are shorter than that for the PS II preparation itself. The lower stability of the sensors compared to protein sample is probably caused by Ag^+ ions released from the reference electrode, which are toxic for the PS II activity. This could be improved by increasing a spatial separation of the working and reference electrode. Thus, the Ag^+ ions released from the reference electrode would not come into contact with the PS II particles immobilized on the working electrode. However, this would make the measurement less practical.

Table 4.2.1: Chlorophyll content from spectra in Figure 4.2.1

	[Chl <i>a</i>] /(mg/mL)	[Chl <i>b</i>] /(mg/mL)	[Total Chl] /(mg/mL)	A_{675}/A_{645}
BBY	2.0	0.9	2.9	2.9
Thylakoid	1.9	0.8	2.7	3.5
BBY before Triton treatment	1.5	1.1	2.6	2.0
Thylakoid before sonication	1.4	1.5	2.9	1.4

Figure 4.2.2 compares the photocurrent signals from the biosensor with

immobilized thylakoid membrane (A) and BBY membrane (B). The signals are registered with FeCy used as a mediator to transfer the electrons from the PS II to the electrodes. The working electrode was polarized at 0.36V to the reference electrode. Both signals were obtained upon illumination for a period of 20 sec and with the sensitivity set to 1 nA. The signal amplitude is calculated by subtracting the average baseline from the readings.

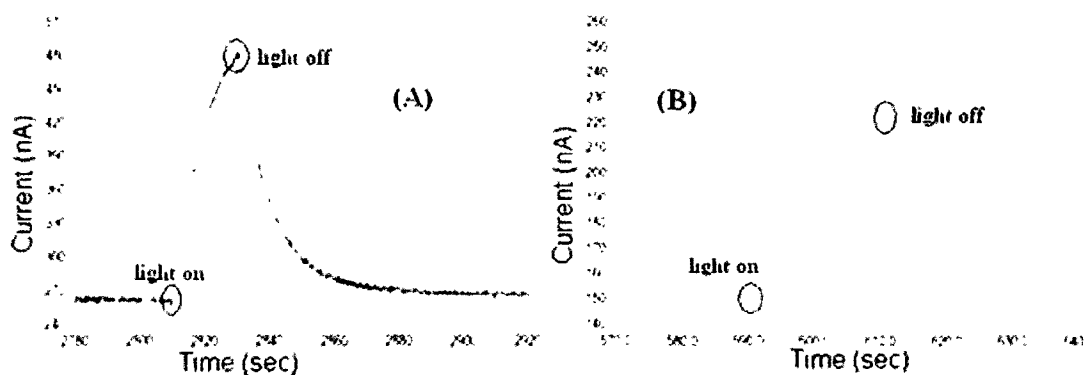


Figure 4.2.2: Photo-current signals of biosensor employing (A) thylakoid membrane and (B)BBY membrane
The signals are registered with FeCy used as a mediator.

The signal amplitude in Figure 4.2.2(A) is 210 nA, which is twice large as the amplitude of the BBY signal, despite the fact that the specific oxygen activities of the two types express the opposite tendency. A possible explanation is, that, because the concentration of the detergent used is 25 times of Chl in the preparation, in the presence of high-concentrated non-ionic detergent, the effective concentration of Fe^{3+}

in the measuring solution is decreased.

Besides the signal amplitude, the response speed is also crucially important to the performance of the biosensor. The ideal photo-current signal should be as shown in Figure 3.4.2. In Figure 4.2.2 (A), the current reaches the peak 20 sec after the light is switched on, and recovers to the baseline in 30 sec after the end of the illumination; secondly, it shows that the background is noisy and the signal current fluctuates. In the case of BBY sample, the signal rises to the peak and recovers to the baseline within just several seconds after the switching of the light on or off; the signal exhibits low noise, and better repeatability.

Table 4.2.2 shows the data derived from Figure 4.2.2. Only the peak-signal generation part was taken into account when calculating the signal RMS amplitude. The SNR of BBY sample is 10000, which is 23 times larger than for thylakoid samples.

Table 4.2.2: Photocurrent signal performance of biosensors immobilized with thylakoid membrane and BBY membrane.

	Peak-signal Generation (sec)	Peak-signal Degeneration (sec)	Signal RMS Amplitude (nA)	Noise RMS Amplitude (nA)	SNR
Thylakoid	20	30	148.5	7.07	441
BBY	4	6	70.7	0.7	10000

By jointly considering the factors including signal amplitude, signal-responsibility and SNR, it is thus safe to say that the BBY-based biosensor exhibits better sensitivity than thylakoid membrane-based biosensor. The differences of sensitivity and fluctuation between thylakoid and BBY samples are apparently due to the activity and purity. The existence of other proteins and complexes in thylakoid membrane limits the effective electron transfer from the PS II comparing to the case of BBY, and makes the signal to noise ratio poorer as well. Summarizing, BBY sample appears to be more suitable for the biosensor application.

4.3 Optimization of biosensor activity

The detergent solubilization during the preparation of BBY membranes may cause some rearrangement of the acceptor side of PS II. The entrapment of BBY membranes by BSA-glutaraldehyde matrix is also possible to interfere with the photosynthesis.

To ensure that these effects do not affect PS II significantly, a measurement of photocurrent depending on wavelength was performed at 25°C in the presence of 0.2mM of DQ in the pH 6.5 measuring buffer (Figure 4.3.1). The maximum activity was obtained at 675 nm and the activities at other wavelengths show a decline, which is as expected assuming that the absorption spectrum of PS II has not changed as a result of biosensor preparation. This wavelength dependence measurement proves that the detergent preparation method and the immobilization procedure with BSA-glutaraldehyde keep the PS II complex reasonably intact and active. The illumination

wavelength was set at 670 nm for the electrochemical experiments.

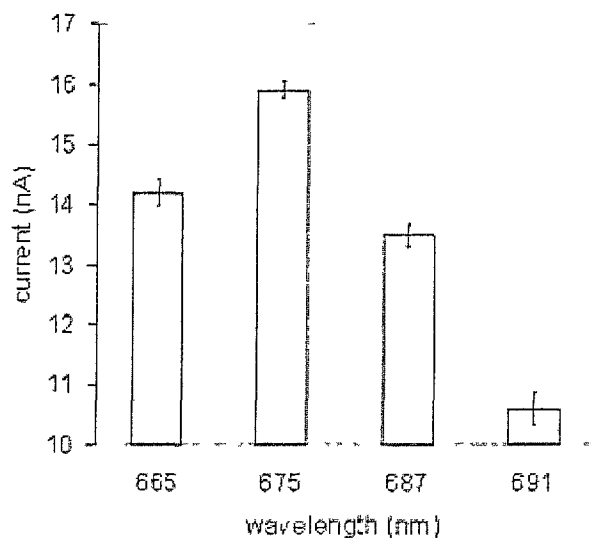


Figure 4.3.1: Wavelength dependence of photocurrent signals of the BBY-based biosensor

Photocurrent signals are measured upon illumination by laser at different wavelengths at 25°C in the presence of 0.2mM of DQ in the measuring buffer.

It is also important to select the appropriate mediator for the measurement. FeCy and DQ were chosen due to their moderate affinity for the Q_B binding site on D1. In other words, they are not expected to displace explosive/herbicide from the Q_B binding site [63].

In the presence of FeCy as a mediator, the biosensor exhibits about three times higher signals as compared to the signals obtained with DQ. This is apparently due to the higher concentration of electron acceptor in use. However, the relatively high oxidizability of FeCy may affect the inhibition in two possible ways. First, in the presence of FeCy, there exists an alternative herbicide-insensitive pathway of PS II

reoxidation bypassing the Q_B pocket and operating at 50% of the rate in the absence of herbicides. It was found that about 50% of the biosensor activity could not be blocked when FeCy was used for the detection of herbicide by Koblizek et al [9]. Secondly, nonheme iron can be slowly oxidized by FeCy, resulting in the reduction of binding affinity of herbicides to the Q_B site [64, 65]. This negatively affects the reproducibility and sensitivity of the biosensor. In contrast, DQ can accept electrons only via the Q_B pocket [63, 66]; and does not react with other components in the PS II reaction center. Therefore DQ was considered better suited for the detection of herbicide/explosive.

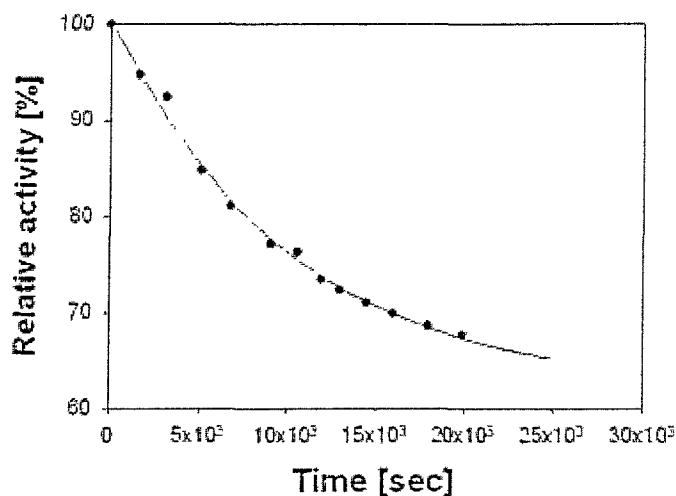


Figure 4.3.2: Time dependence of stability of the biosensor
Relative activities of BBY membranes immobilized on biosensor are measured at 25°C in the presence of 0.2mM of DQ in the measuring buffer. The 100% value represents the maximal activity obtained in the measurement.

According to the conclusion from the paragraph above, BBY-based biosensor was used with DQ as mediator in the subsequent measurement. The time dependence of

stability of the biosensor using BBY membranes at 25°C in the presence of 0.2mM of DQ was obtained in the pH 6.5 measuring buffer (Figure 4.3.2). The activity of the PS II particles decreases with time in an exponential way with 70% of the biosensor activity remaining after 3 hours.

4.4 Results of detection with the biosensor

For detection of the explosive/herbicide the biosensor was subjected to a droplet containing the analyte, and the light induced current change was measured after 15 minutes to stabilize the system. This incubation time has been previously judged necessary in case of BSA-glutaraldehyde immobilization as the analyte molecule has to diffuse to its binding site and that process is slow for the gel-matrix system [67]. Before applying next, higher, concentration of analyte, the sensor was treated with the pH 6.5 measuring buffer. Alternatively, a fresh sensor was used to obtain the response at a particular analyte concentration in case of otherwise unreproducible detection. On starting the measurements with a new biosensor the background current was higher and the photocurrent signal measurements showed higher standard deviations during the first 30 min of the measurement. This may be referred to as a preconditioning phase after which the measurement becomes more stable. Thereafter the signal was largely stable over a period of 3 hours during which the different concentrations could be tested using 15 min incubation time.

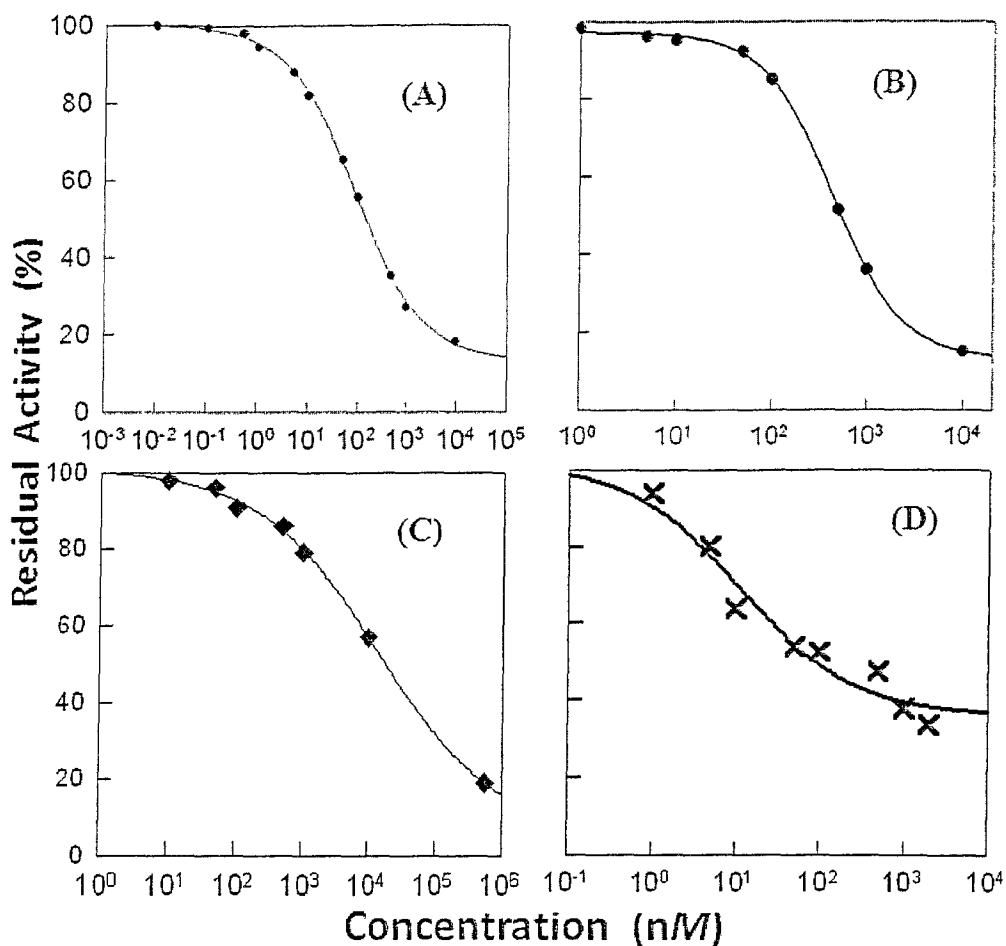


Figure 4.4.1: Binding curves of DCMU and explosives in the presence of 0.2mM DQ (A) DCMU; (B) Picric acid; (C) TNT; (D) tetryl. The residual activity (in %) was calculated as the ratio of signals in the presence/absence of the herbicide. The experimental points were fitted using equation 3.5.1 yielding the EC50 values of $8.8 \times 10^{-8} M$ for DCMU ($R^2=0.999$), of $4.4 \times 10^{-7} M$ for picric acid ($R^2=0.999$), of $1.4 \times 10^{-5} M$ for TNT ($R^2=0.997$) and of $1.1 \times 10^{-8} M$ for tetryl ($R^2=0.985$).

The ratio of the signals in the presence and absence of analyte was plotted against analyte concentration (Figure 4.4.1). Binding curves for each analyte were analyzed using the half-maximal effective concentration (Equation 3.5.1), which was specified in section 3.5. The LOD was determined on the basis of 99% confidence interval,

which, assuming the normal distribution, corresponds to $2.6 \times$ standard error of the measurement (σ). The calculation results are shown in Table 4.4.1.

As can be seen from Figure 4.4.1 the resulting curves follow a sigmoidal tendency. The biosensor is highly responsive to a classical herbicide such as DCMU and only slightly less responsive to picric acid and tetryl. Essentially, the sigmoidal curve shifts towards higher concentration for picric acid and tetryl, and shifts even further for TNT. The range of recognition for DCMU is from 10^{-3} nM to $10 \mu M$, for picric acid and tetryl is from 1 nM to $1 \mu M$. The small recognition range of picric acid is due to the low SNR for concentrations higher than $1 \mu M$. The standard error is related to the SNR of the measurement. The high standard error of tetryl can explain the small recognition range. In the case of TNT the biosensor shows no inhibition of photocurrent for concentrations up to 10nM, but the inhibition effect becomes apparent upon further increasing the TNT concentration.

Table 4.4.1: Detection results based on binding curves in Figure 4.4.1

	EC50 (M)	LOD (M)	R^2	σ	Hill slope
DCMU	8.8×10^{-8}	2×10^{-9}	0.999	0.9245	0.631
Picric acid	4.4×10^{-7}	1×10^{-8}	0.999	1.1254	1.217
tetryl	1.1×10^{-8}	2×10^{-9}	0.985	5.2936	0.648
TNT	1.4×10^{-5}	7×10^{-7}	0.997	1.8379	0.476

The value of EC50 obtained coincides with the PS II-inhibitor dissociation constant according to the Langmuir adsorption isotherm. The high EC50 indicates a weak binding to the Q_B site. The EC50 of DCMU obtained is $8.8 \times 10^{-8} M$, which is very close to the result reported by Koblizek et al [9] using a flow-cell set-up. Tetryl exhibits EC50 of $1.1 \times 10^{-8} M$ indicating a high binding affinity. The effective inhibition by TNT takes place at high concentration only (EC50 is $1.4 \times 10^{-4} M$) suggesting that TNT binding to the Q_B is weak.

The Hill slope coefficient is an interesting parameter which is related to the cooperativity of a ligand binding. The slope factor describes the steepness of a curve. In most situations, there is no straightforward way to interpret the numerical value of the Hill slope coefficient in terms of chemistry or biology. Qualitatively, if the Hill slope coefficient is far from 1.0, the binding does not follow the law of mass action with a single site. The reasons for the reduced Hill slope coefficient may include the presence of several clustered binding sites with somewhat different affinities, but since the value of the Hill slope is very sensitive to experimental and curve fitting problems, we refrain from making any far-reaching conclusions.

Compared to the detection limit of the biosensor system developed by Koblizek et al. [9], this droplet biosensor performs quite well. The LOD of picric acid previously reported using the luminescence quenching method is $2 \times 10^{-6} M$ [68] and by fluorescence emission of hexaphenylsilole-chitosan film as 21 nM [69]. Thus, the present detection limit for picric acid of $8 \times 10^{-9} M$ exhibits a significant improvement over luminescence quenching, but is comparable to that of the fluorescence detection

method. The LOD of DCMU, picric acid and tetryl are at nM range with only TNT being an exception. In the following we attempt to explore possible reasons for such a low sensitivity for TNT.

In general, the sensitivity and the detection limit of the biosensor are determined by the chemical structure of the inhibitor and by the architecture of the Q_B pocket [48], but are also related to the design of the biosensor and the characteristics of the immobilization system especially at low concentrations of inhibitors. Effort has been made to optimize the latter parameters. First, the PS II particles applied have higher specific activity compared to thylakoid membranes. Second, the BSA-glutaraldehyde matrix results in a very stable entrapment of PS II particles on the surface of the working electrode. This set-up assures a high concentration of active PS II complexes in the micro-environment around the electrode, which in turn, results in a good, stable signal. Nevertheless there is a possibility that permeability of the BSA-glutaraldehyde matrix to TNT is low for some reason and therefore the inhibition effect is decreased. The logic behind the use of Langmuir adsorption isotherm assumes an excess of the free compound with respect to the number of binding sites. Thus, the accessibility of TNT to the electrode surface and to the PS II is critical for detection, especially when it's at low concentration.

Results derived from other methods such as the DCPIP assay will be discussed in the following section to further explore the binding of TNT.

4.5 Supplemental studies of TNT

Detection of TNT was also explored in the presence of FeCy (instead of DQ) because of the high SNR and amplified signal currents. Figure 4.5.1 depicts the respective binding curve. As expected, the binding curve shows an incomplete inhibition at the saturated concentration of TNT (residual activity 40%) due to the properties of FeCy as described above. The residual activity in Figure 4.4 (C) at the maximal concentration is about 20%. The EC50 ($5.4 \times 10^{-5} M$) and LOD ($4.7 \times 10^{-7} M$) are similar to the result from the detection in the presence of DQ. So far it proves that the detection of TNT with both types of mediators has similar sensitivity.

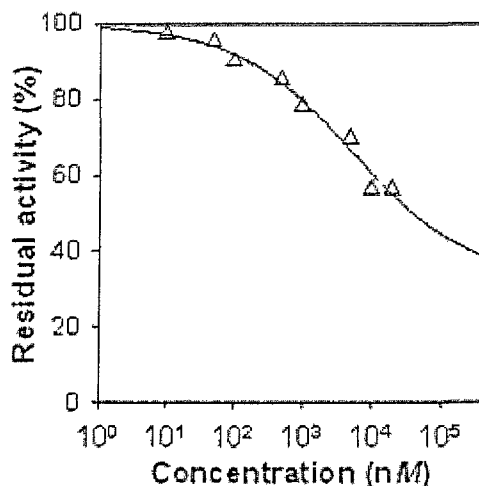


Figure 4.5.1: Binding curves of TNT in the presence of 1mM FeCy. The experimental points were fitted using equation 3.5.1 yielding the EC50 values of $5.4 \times 10^{-6} M$ ($R^2=0.990$).

To clarify the effect of BSA-glutaraldehyde matrix on TNT, a DCPIP assay was employed as a supplementary method. The rate of photoreduction of DCPIP was measured depending on the increase of TNT concentration in the pH 7.5 measuring buffer with DCPIP as the electron acceptor. The residual activity of PS II is equal to the ratio of the photoreduction rate in the presence of TNT to that in the absence of TNT. Experimental details have been illustrated in Section 3.2. The binding curve was fitted by Equation 3.5.1. The resulting EC50 is $3.7 \times 10^{-5} M$ and LOD is $4.4 \times 10^{-6} M$. This sensitivity and binding affinity slightly declined with respect to those shown in Table 4.4.1 indicating that the choice of a matrix system does not pose significant limitations to the interaction of TNT with the PS II complex.

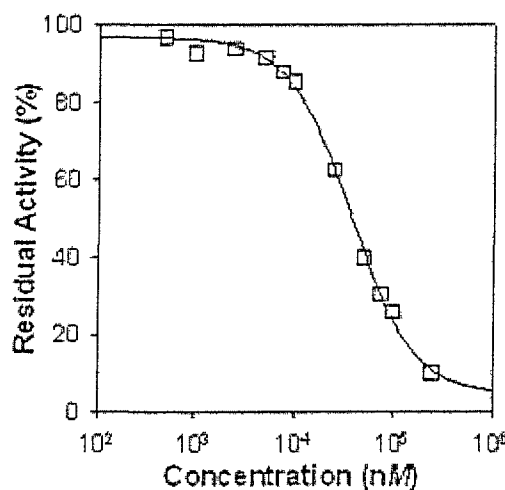


Figure 4.5.2: Binding curve of TNT-DCPIP assay
 Photoreduction rate is calculated as the decrease of DCPIP significant absorption peak (~ 600 nm) over illumination time. Residual activity equals to the ratio of the photoreduction rate in the presence of TNT to that in the absence of TNT.

There are some differences between the two curves for TNT in biosensor detection

and in DCPIP assay. The DCPIP assay is not responsive to low concentration of TNT up to $10^{-6}M$, and the inhibition is almost complete for a saturated solution of TNT (solubility of TNT is $5.7 \times 10^{-4}M$). This is due to the significant difference of measuring environment. The concentration of PS II in the solution is $\sim 2 \times 10^{-7}M$ (0.5 to 1 μg Chl, $\sim 10^{-11}$ mol PS II) in DCPIP assay, whereas on the electrode it is $10^{-5}M$. At low concentration of TNT, the photoreduction rate is too low to be recorded. However, the relatively high ratio of TNT to PS II makes the inhibition more completed at high TNT concentration. The natural decomposition of PS II during the spectroscopic measurement may be responsible for the activity loss as well.

As mentioned in Chapter 1, TNT is known to have an inhibitory effect on plant growth. High concentration of TNT in soil has been shown to be toxic and increase non-photochemical energy dissipation [23]. Thus, the question may be posed if the inhibition shown in Figure 4.4 (C), Figure 4.5.1 and DCPIP assay is a result of permanent damage caused by TNT to the PS II. Figure 4.5.3 shows the photocurrent response of BBY-based biosensor in the presence of FeCy, to the saturated TNT solution, i.e. the maximum concentration possibly achievable in the experiments on whole plants. The first two peaks were obtained in the absence of TNT for reference. The photocurrent is reduced to nearly zero when saturated solution of TNT is added (arrow-pointed small peak). Washing the electrode surface with pH 6.5 buffer completely (although gradually) restores the magnitude of the photocurrent.

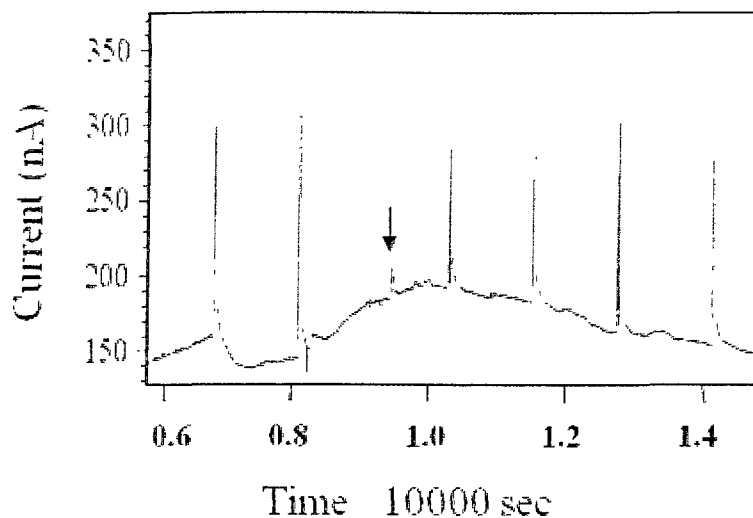


Figure 4.5.3: Recoverability of biosensor after the detection of TNT
 The photocurrent signals are measured in the presence of FeCy. The first two peaks were obtained in the absence of TNT. Saturated TNT solution was added (small arrow) to observe the recovery of the photocurrent.

The same regeneration experiment for the biosensor employed for tetryl detection yielded only 50% of photocurrent recovery (data not shown). Although tetryl inhibits the PS II activity at very low concentrations as shown in Figure 4.4 (D), the ligand-binding effect is not fully reversible, indicating permanent damage to the PS II. Therefore the biosensor for the detection of tetryl is of low reproducibility.

The above supplementary experiments on TNT exclude the environmental factors and prove that TNT binding to PS II is reversible. Thus, the question of low sensitivity of our biosensor to TNT narrows down to the chemical properties of TNT and its interaction with the Q_B pocket. One conceivable explanation is, that, TNT binds on some site other than Q_B without interrupting the electron transport of PS II.

This extra binding has to be reversible, and exceed the binding affinity for the TNT- Q_B binding. It is difficult to predict the potential binding site considering that TNT is a very small ligand compared to the size of PS II complex. Second, because of the high hydrophobicity of TNT molecule, it is possible that the hydrophobic components of the membrane block TNT from contact with the acceptor-side on PS II. Note that both biosensor and DCPIP assay experiments were performed with PS II particles still retaining the membrane/detergent environment.

Chapter 5

Molecular modeling of inhibitors binding to PS II

The detection results show a higher inhibition effect for nitric explosives such as tetryl and classical herbicides such as DCMU, with the effect slightly decreasing for picric acid and further strongly decreasing for TNT. It would appear that the occurrence of a $-\text{CH}_3$ group in TNT instead of $-\text{OH}$ group should pose significant limitations to the ability of TNT to bind to the Q_B site, as sufficient number of hydrogen bonds cannot be formed. To test this hypotheses molecular modeling of binding of the inhibitors to the Q_B binding site was performed using Autodock Vina [70].

5.1 Introduction to Autodock

AutoDock is a program designed to predict how small molecules bind to a receptor of known 3D structure. It is a suite of automated docking programs: AutoTors, which facilitates the input of ligand coordinates; AutoGrid, which precalculates a three-dimensional grid of interaction energy based on macromolecular coordinates; and

AutoDock, which performs the docking simulation [71]. These programs are linked by a host of shell scripts to streamline the input of new structures, to launch AutoDock simulations in parallel on a cluster of machines, and to facilitate the analysis of results. A simulated annealing algorithm is used for searching conformations, allowing several torsional degrees of freedom in a flexible ligand to be searched during the docking experiment, but with the limitation that it may not always find the global minimum conformation. A grid-based technique is used for energy evaluation at each step of the simulation, providing a detailed energetic model at reasonable computational cost, but carrying with it the restriction of a rigid protein target. The computation assumes that protonation state of and charge distribution in the molecules do not change between, e.g., their bound and unbound states. The docking results in reproducing chemical potentials, which determine the bound conformation preference and the free energy of binding. It combines the consideration not only of the minima in the energy profile but also of the shape of the profile and the temperature. The energy profile includes evaluations of dispersion/repulsion, hydrogen bonding, electrostatics, and desolvation.

AutoDock Vina is the latest version of Autodock released in 2010. It has significantly improved speed of computation and the accuracy of the binding mode predictions. With a command-based operation, AutoDock Vina automatically calculates the grid maps and clusters the results in a way transparent to the user.

5.2 Docking of inhibitors by AutoDock Vina

The receptor used in AutoDock Vina is a modified PS II PDB file downloaded from RCSB Protein Data Bank (PDB entry: 3bz1 [72]). This file contains the X-ray crystallography data of dimeric PS II obtained from cyanobacterium *Thermosynechococcus elongatus* (X-ray structure of PS II of spinach is not available yet) at 2.9 Å resolution, in which D1 subunit is coded as chain A. Plastoquinone molecule (code: PL9) on chain A was extracted by Pymol manually and saved as a ligand for future simulations. The PDB files of other ligand molecules are prepared by online software CORINA (Molecular Networks). For both the receptor and the ligands, Autodock Tools (ADT) 1.5.4 was used to add hydrogens (polar and non-polar) and compute Gasteiger charges. Torsions of the ligands were optimized by ADT automatically, except for the long side chain of plastoquinone whose bonds were assumed to be non-rotatable bonds to simplify the computation. The center of the grid box was set at the center of Q_B pocket, which has been described in detail in section 2.5. The grid map parameters are as followed:

Grid Box center: X=22.66, Y=62.917, Z=32.6

Grid Box size: X=25, Y=25, Z=25

Grid spacing =1.0 Å

5.2.1 Docking of Plastoquinone

Modeling proper docking of a plastoquinone to the Q_B site was not successful in our case. As a matter of fact, there has not been any report of successful simulation of plastoquinone- Q_B docking so far. Takahashi et al. [73] have performed a structural optimization of the Q_B site, including the non-heme iron, Q_B , and surrounding amino acids using molecular mechanics calculations. By cutting down the numbers of carbons in the side chain, the modified plastoquinone can be simulated as located at both ends of the Q_B pocket: either near the imidazole of HIS215 at one end, or near the -OH group of SER264, the backbone -NH- group of PHE265, and the backbone -CO group of ALA263 at the other end (see Figure 5.2.1). The binding affinity wasn't given in Takahashi et al [73].

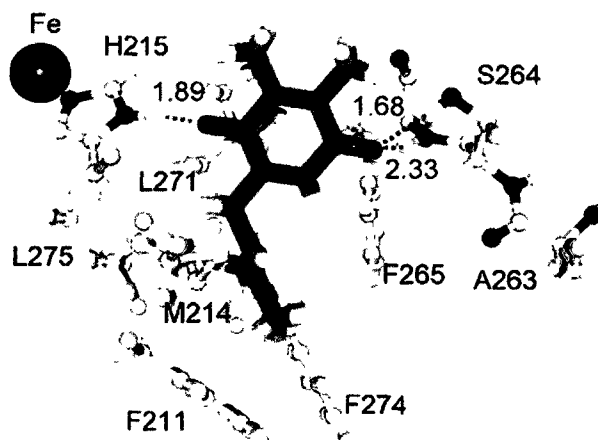


Figure 5.2.1: Model of binding site of PQ in the Q_B pocket by Takahashi et al.

The long side chain on plastoquinone makes it very difficult to fit into the pocket spontaneously. The best-scored docking results by Autodock Vina shows that plastoquinone molecule with flexible side chain can bind to SER264 and PHE265 outside the Q_B pocket with a binding affinity of 148 kcal/mol. Therefore, according to simulations, the binding of plastoquinone on Q_B site in vivo is not spontaneous.



Figure 5.2.2: Binding of PQ in the Q_B pocket of PS II

Figure 5.2.2 depicts the original conformation of plastoquinone in the pocket of PS II (PDB entry: 3bz1) analyzed by Pymol plug-ins. Plastoquinone is shown in green sticks in the center of both Figures 5.2.1 and 5.2.2. Hydrogen bonded residues are labeled by residue names and shown with hydrogens added. Hydrogen bonds are shown in dashes with bond lengths labeled in Å. Some residues in the cartoon structures are hidden for the purpose of clarity. As mentioned above, the

plastoquinone of chain A (D1) is coded by PL9 in 3bz1. Only the quinone part (the head side of the molecule) is located in the pocket. In this pocket, one of the -CO groups of plastoquinone is hydrogen-bonded to HIS215 and the other -CO group interacts with the -OH group of SER264 and the backbone -NH- group of PHE265. The bond-lengths of these polar contacts (2.8 Å) from the original X-ray structure indicate that the binding in vivo are much weaker than the binding from the docking results done by Takahishi et al.

5.2.2 Docking of explosive molecules

The docking conformations of picric acid, TNT and tetryl are shown in Figure 5.2.3, Figure 5.2.2 and Figure 5.2.5 respectively. AutoDock Vina outputs results containing 9 ligand conformations in the specified grid scored by binding affinity. The resulting PDBQT type files were first processed in AutoDock Tools to separate into individual molecules and to add hydrogen, then analyzed by Pymol. The residues on chain A within 4.0 Å of the ligand were selected. The manually refined selected residues structure the binding pocket. The color codes for the atoms are: C-green, H-white, O-red, N-blue, Cl-green.

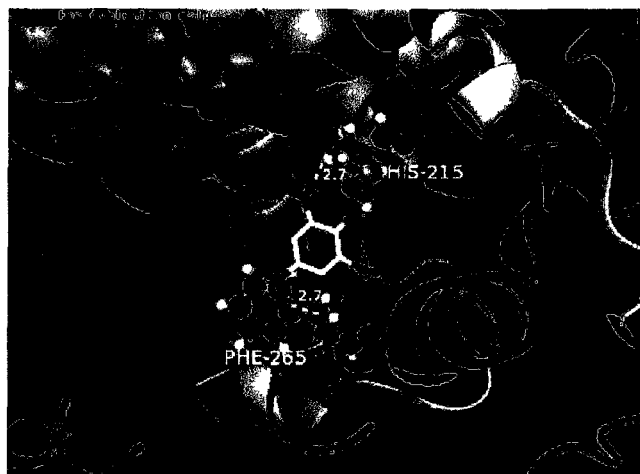


Figure 5.2.3: Binding of picric acid in the Q_B pocket of PS II

Picric acid binds to the Q_B binding site by two hydrogen bonds according to the docking results. One nitro group of picric acid binds to the backbone $-NH-$ group of PHE265 with a bond-length of 2.7Å ; another $-NO_2$ group binds to the imidazole of HIS215 with a bond-length of 2.7Å . The binding affinity calculated by Autodock Vina is -6.4 kcal/mol . The binding pocket of picric acid comprises of residues: PHE211, MET214, HIS215, LEU218, HIS252, PHE255, ILE259, TYR262, ALA263, SER264, PHE265 and LEU275.

Figure 5.2.4(a) shows that TNT binds on the Q_B binding site by two hydrogen bonds. Two of the TNT nitro groups bind to the backbone $-NH-$ group of PHE265 and the $\delta-N$ of HIS215, respectively. Both bond-lengths equal to 2.7Å . The binding affinity is -6.8 kcal/mol . The residues in the binding pocket are: PHE211, MET214, HIS215, LEU218, VAL219, TYR246, ILE248, ALA251, HIS252, PHE255, ILE259, ALA263, SER264, PHE265, LEU271, PHE274.



(a) Binding of TNT in the Q_B pocket of PS II



(b) Binding of TNT on chain C of PS II

Figure 5.2.4: Two models of binding of TNT on PS II

(a) Binding of TNT in the Q_B pocket of PS II , (b) Binding of TNT on chain C of PS II

Another competitive binding site of TNT on PS II was found on Chain C, the light harvesting subunit CP43 (Figure 5.2.4(b)). The binding affinity of this docking result is -6.8 kcal/mol. One hydrogen bond (2.2 Å) is built between nitro group of TNT and residue LYS79, while another hydrogen bond (2.7 Å) is between another $-NO_2$ group and ASN418.

Although the effect of this binding of TNT to the CP43 subunit is not clear so far, it can possibly consume the TNT molecules in the solution so that the effective TNT concentration to which the Q_B binding site is exposed is decreased. However, this one site is obviously not enough to explain our observations. In the detection of TNT and picric acid by biosensors, the EC_{50} values imply that TNT should have much lower binding affinity than picric acid. Apparently, the presence of another, yet undiscovered binding site with higher binding affinity offers a reasonable explanation.



Figure 5.2.5: Binding of tetryl in the Q_B pocket of PS II

The best docking result presented in Figure 5.2.5 of Tetryl has a binding affinity of -5.0 kcal/mol. Two oxygen atoms on the $-NO_2$ of tetryl bind to the backbone $-NH-$ group of SER264 and PHE265 respectively. Both of the bond-lengths are 2.3 Å. The pocket ring of tetryl on PS II contains residues: PHE211, MET214, HIS215, LEU218, HIS252, PHE255, ILE259, TYR262, ALA263, SER264, PHE265, LEU271,

PHE274, LEU275.

5.2.3 Docking of herbicide molecules



(a) Binding of DCMU through -NH- group in the Q_B pocket of PS II



(b) Binding of DCMU through -CO group in the Q_B pocket of PS II

Figure 5.2.6: Two models of binding of DCMU in the Q_B pocket
(a) Binding of DCMU through -NH- in the Q_B pocket of PS II, (b) Binding of DCMU through -CO in the Q_B pocket of PS II

We also simulated the docking of herbicides, i.e. DCMU and atrazine to compare with the results obtained above for explosives. DCMU exhibits two ways of binding to PHE265 on D1. As shown in Figure 5.2.6(a), the $-NH-$ group of DCMU interacts with $-CO$ of PHE265 by hydrogen bond. The binding affinity in this case is -7.1 kcal/mol, In Figure 5.2.6(b), $-CO$ group of DCMU binds to the $-NH-$ of PHE265, resulting in a binding affinity of -6.7 kcal/mol. These two binding have the same bond-length (2.5 \AA) and are both located inside the Q_B pocket.

Still another possibility is similar to the docking calculated by Takahashi et al. [73], in which the simulated binding for DCMU was on SER264 through the $-CO$ group in a trans-amide conformation without any interaction with HIS215. The residues related to the binding are: PHE211, MET214, HIS215, LEU218, PHE255, SER264, PHE265, LEU271, PHE274.



Figure 5.2.7: Binding of atrazine in the Q_B pocket of PS II

The binding affinity of atrazine (-6.5 kcal/mol) is smaller than that of DCMU, even though two hydrogen bonds are found. The nitrogen atom on the triazine ring binds to -NH- of PHE265 with a distance of 2.2 Å. The other hydrogen bond that is 2.5 Å takes place between the -NH- of atrazine and -CO group of PHE265. The binding pocket derived from this docking is: PHE211, MET214, HIS215, LEU218, ALA251, HIS252, PHE255, ALA263, SER264, PHE265, LEU271, PHE274.

5.2.4 Discussion of docking results by AutoDock

The studies of *Synechococcus* PCC7942 showed that SER264 was essential for binding of atrazine, DCMU and quinone [74]. Instead of SER264, we found that PHE265 is playing an important role in the docking. Here we were using the X-ray crystallography data of PS II isolated from *Thermosynechococcus elongatus*. This is due to the difference of protein structures from different strains of cyanobacteria. The crystal structure of 3bz1 shows that the -OH group of SER264 faces to the exterior side of the Q_B pocket, so that the backbone -NH- group of PHE265 is more likely to get involved in the binding of amides in this case.

According to earlier research of herbicide-resistant mutants, most types of herbicides (i.e., urea type DCMU and triazine type atrazine) lean toward the SER264 side, and phenolic type herbicides toward the HIS215 side of the Q_B pocket [15, 48]. Since those studies were done before high resolution X-ray structure of PS II became available, the model was based on the reaction center of purple photosynthetic bacteria, in which L and M subunits are homologies of D1 and D2 in PS II. In

the case of *Thermosynechococcus elongatus*-based model, atrazine and DCMU bind at the PHE265 side as shown in Figures 5.2.7 and 5.2.6(b). We also found the similar preference for binding orientation in the case of explosives. For instance, picric acid, as a phenolic compound, interacts with HIS215 and PHE265 in Figure 5.2.3.

Binding affinity and dissociation constant are two reciprocal properties of ligand-protein binding, although they are from different expressions of binding equilibrium. The dissociation constant is the concentration needed to get half-maximal occupancy of the binding site. Thus, lower EC50 in our case means it takes less to get the same amount of binding - this is what one thinks of for higher affinity or stronger binding. We didn't find any relevant relationship between the binding affinity calculated by AutoDock Vina and the experimental dissociation constant in Table 5.2.1. This is most likely due to the limitation of AutoDock in considering the solvent effect. Nevertheless, it offers a technique to predict the potential conformation of binding.

Table 5.2.1: Modeling results of the PS II inhibitors binding to the Q_B pocket

	Binding Pocket	Binding Affinity of Docking Results (kcal/mol)	Dissociation constant (EC50) <i>M</i>
PQ	<i>PHE211, MET214, HIS215, LEU218, ALA251, HIS252, PHE255, SER264, PHE265, LEU271</i>	—	—
Picric acid	<i>PHE211, MET214, HIS215, LEU218, HIS252, PHE255, ILE259, TYR262, ALA263, SER264, PHE265, LEU275</i>	-6.4	1.5×10^{-7}
TNT	<i>PHE211, MET214, HIS215, LEU218, VAL219, TYR246, ILE248, ALA251, HIS252, PHE255, ILE259, ALA263, SER264, PHE265, LEU271, PHE274</i>	-6.8	1.4×10^{-5}
Tetryl	<i>PHE211, MET214, HIS215, LEU218, HIS252, PHE255, ILE259, TYR262, ALA263, SER264, PHE265, LEU271, PHE274, LEU275</i>	-5.0	1.1×10^{-8}
DCMU	<i>PHE211, MET214, HIS215, LEU218, PHE255, SER264, PHE265, LEU271, PHE274</i>	-6.7	8.8×10^{-8}
Atrazine	<i>PHE211, MET214, HIS215, LEU218, ALA251, HIS252, PHE255, ALA263, SER264, PHE265, LEU271, PHE274</i>	-6.5	3×10^{-7} *

* The EC50 of atrazine is from the detection of herbicides by Koblizek et al. [9].

Chapter 6

Conclusion

A biosensor based on Photosystem II-enriched particles from spinach leaves and inexpensive commercially available screen-printed electrodes has been developed. The biosensor with BBY particles immobilized with BSA-glutaraldehyde is capable of electrochemical detection of not only herbicides but also some explosives. The present biosensor also may be employed in environmental protection applications for rapid screening of picric acid in water samples in a few minutes. While picric acid and tetryl were detected in concentrations similar to those of the widespread herbicides (and with similar concentration dependence likely indicating Q_B site binding), the limits of detection for TNT were significantly higher (worse). Extensive modeling of herbicide and explosives binding to the Q_B binding site of the Photosystem II has been performed, yielding almost identical binding affinities for all compounds studied (except original plastoquinone). In other words, there was no meaningful correlation between the modeling results and measured inhibitory activity. Determination of the other possible reasons for low sensitivity of the PS II-based biosensor to TNT requires

extended research, including that involving isolated bacterial reaction centers as well as other types of explosives resembling different classes of herbicides (e.g. RDX versus atrazine).

Bibliography

- [1] J. V. Goodpaster and V. L. McGuffin. Fluorescence quenching as an indirect detection method for nitrated explosives. *Analytical Chemistry*, 73(9):48824–1322, 2001.
- [2] K. J. Albert and D. R. Walt. High-Speed Fluorescence Detection of Explosives-like Vapors. *Analytical Chemistry*, 72(9):1947–1955, 2000.
- [3] J. S. Yang and T. M. Swager. Fluorescent porous polymer films as TNT chemosensors: Electronic and structural effects. *Journal of the American Chemical Society*, 120(46):11864–11873, 1998.
- [4] A. Rose, Z. Zhu, C. F. Madigan, T. M. Swager, and V. Bulovic. Sensitivity gains in chemosensing by lasing action in organic polymers. *Nature*, 434:876–879, 2005.
- [5] D. R. Shankaran, K. V. Gobi, T. Sakai, K. Matsumoto, K. Toko, and N. Miura. Surface plasmon resonance immunosensor for highly sensitive detection of 2,4,6-trinitrotoluene. *Biosensors and Bioelectronics*, 20(9):1750–1756, 2005.
- [6] R. S. Burlage, D. R. Patek, and K. R. Everman. *Method for detection of buried explosives using a biosensor*, 1999.
- [7] M. Campas, R. Carpentier, and R. Rouillon. Plant tissue- and photosynthesis-based biosensors. *Biotechnology Advances*, 26(4):370–378, 2008.
- [8] M. T. Giardi, M. Koblizek, and J. Masojidek. Photosystem II-based biosensors for the detection of pollutants. *Biosensors and Bioelectronics*, 16(9-12):1027–1033, 2001.

- [9] M. Koblizek, J. Maly, J. Masojidek, J. Komenda, T. Kucera, M.T. Giardi, A.K. Mattoo, and R. Pilloton. A biosensor for the detection of triazine and phenylurea herbicides designed using photosystem II coupled to a screen-printed electrode. *Biotechnology and Bioengineering*, 78(1):110–116, 2002.
- [10] M. Koblizek, J. Masojidek, J. Komenda, T Kucera, R. Pilloton, A. K. Mattoo, and M. T. Giardi. A sensitive photosystem II-based biosensor for detection of a class of herbicides. *Biotechnology and Bioengineering*, 60(6):664–669, 1998.
- [11] C. Jian and W. R. Seitz. Membrane for in situ optical detection of organic nitro compounds based on fluorescence quenching. *Analytica Chimica Acta*, 237:265–271, 1990.
- [12] H. H. Zeng, K. M. Wang, C. L. Liu, and R. Q. Yu. A reversible optode membrane for picric acid based on the fluorescence quenching of pyrene. *Talanta*, 40(10):1569–1573, 1993.
- [13] C. G. Niu, Z. Z. Li, X. B. Zhang, W. Q. Lin, G. L. Shen, and R. Q. Yu. Covalently immobilized aminonaphthalimide as fluorescent carrier for the preparation of optical sensors. *Analytical and Bioanalytical Chemistry*, 372(4):519–524, 2002.
- [14] X. Yang, C. G. Niu, G. L. Shen, and R. Q. Yu. Picric acid sensitive optode based on a fluorescence carrier covalently bound to membrane. *Analyst*, 126:349–352, 2001.
- [15] W. Oettmeier and K. Masson. Picrate as an Inhibitor of Photosystem II in Photosynthetic Electron Transport. *European Journal of Biochemistry*, 122(1):163–167, 1982.
- [16] E. Ercag, A. Uzer, and Apak R. Selective spectrophotometric determination of trinitrotoluene, trinitrophenol, dinitrophenol and mononitrophenol. *Analytica Chimica Acta*, 505:83–93, 2004.
- [17] E. Ercag, A. Uzer, and Apak R. Selective spectrophotometric determination of TNT using a dicyclohexylamine-based colorimetric sensor. *Talanta*, 78(3):772–780, 2009.

- [18] J. Wannlund and M. Deluca. A sensitive bioluminescent immunoassay for dinitrophenol and trinitrotoluene. *Analytical Biochemistry*, 122(2):385–393, 1982.
- [19] J. Wang, R. K. Bhada, J. Lu, and D. Macdonald. Remote electrochemical sensor for monitoring TNT in natural waters. *Analytica Chimica Acta*, 361(1-2):85–91, 1998.
- [20] H. Sohn, R. M. Calhoun, M. J. Sailor, and W. C. Trogler. Detection of TNT and Picric Acid on Surfaces and in Seawater by Using Photoluminescent Polysiloles. *Angewandte Chemie*, 113(11):2162–2163, 2001.
- [21] K. S. Ro, A. Venugopal, D. D. Adrian, D. Constant, K. Qaisi, K. T. Valsaraj, L. J. Thibodeaux, and D. Roy. Solubility of 2,4,6-Trinitrodoluene(TNT) in water. *Journal of Chemical and Engineering Data*, 41(4):758–761, 1996.
- [22] Y. Ouyang, C. H. Huang, D. Y. Huang, D. Lin, and L. Cui. Simulating uptake and transport of TNT by plants using STELLA. *Chemosphere*, 69(8):1245–1252, 2007.
- [23] N. A. Ali, D. Dewez, P. Y. Robidoux, and R. Popovic. Photosynthetic parameters as indicators of trinitrotoluene (TNT) inhibitory effect: Change in chlorophyll a fluorescence induction upon exposure of *Lactuca sativa* to TNT. *Ecotoxicology*, 15:437–441, 2006.
- [24] R. L. Marple and W. R. LaCourse. Application of photoassisted electrochemical detection to explosive-containing environmental samples. *Analytical Chemistry*, 77:6709–6714, 2005.
- [25] S. D. Harvey, R. J. Fellows, J. A. Campbell, and D. A. Cataldo. Determination of the explosive 2,4,6-trinitrophenylmethylnitramine (tetryl) and its transformation products in soil. *Journal of Chromatography A*, 605(2):227–240, 1992.
- [26] M. M. Shah and J. C. Spain. *Biochemical and Biophysical Research Communications*, 220(3):563, 1996.
- [27] R. Hodyss and J. L. Beaucham. Multidimensional Detection of Nitroorganic Explosives by Gas Chromatography-Pyrolysis-Ultraviolet Detection. *Analytical chemistry*, 77(11):3607–3610, 2005.

- [28] C. A. Timiriazeff. Sur l'action de la lumiere dans la decomposition de l'acide carbonique par la granule de chlorophylle. In *International Botanical Congress*, pages 108–117, Firenze, Italy, 1874.
- [29] R. Emerson and Arnold W. A separation of the reactions in photosynthesis by means of intermittent light. *Journal of General Physiology*, 15:391–420, 1932a.
- [30] S. Govindjee. *Chlorophyll α fluorescence: A bit of basics and history*, pages 1–42. Springer, Dordrecht, 2004.
- [31] L. N. M. Duysens, J. Amesz, and B. M. Kamp. Two photochemical systems in photosynthesis. *Nature*, 190:510–511, 1961.
- [32] K. N. Ferreira, T. M. Iverson, K. Maghlaoui, J. Barber, and S. Iwata. Architecture of the photosynthetic oxygen-evolving center. *Science*, 303:1831–1837, 2004.
- [33] E. P. Fuerst and M. A. Norman. Interactions of herbicides with photosynthetic electron transport. *Weed Science*, 39:458–464, 1991.
- [34] B. Hankamer, J. Barber, and E. J. Boekema. Structure and membrane organization of Photosystem II in green plants. *Annual Review of Plant Physiology and Plant Molecular Biology*, 48:641–671, 1997.
- [35] T. M. Bricker and L. K. Frankel. The structure and function of CP47 and CP43 in Photosystem II. *Photosynthesis Research*, 2002.
- [36] W. P. Schroder and L. X. Shi. The low molecular mass subunits of the photosynthetic supracomplex, photosystem II. *Biochimica et Biophysica Acta*, 1608(2-3):75–96, 2004.
- [37] K. Burda, J. Kruk, R. Borgstadt, J. Stanek, K. StrzaBka, G. H. Schmid, and O. Kruse. Mossbauer studies of the non-heme iron and cytochrome *b559* in a *Chlamydomonas reinhardtii* PSI-mutant and their interactions with alpha tocopherol quinone. *FEBS Letters*, 535:159–165, 2003.
- [38] N. K. Boardman and J. M. Anderson. Isolation from spinach chloroplasts of particles containing different proportions of chlorophyll *a* and chlorophyll *b* and

- their possible role in the light reactions of photosynthesis. *Nature*, 293:166–167, 1964.
- [39] S. Eshaghi, Andersson B., and Barber J. Isolation of a highly active PSII-LHCII supercomplex from thylakoid membranes by a direct method. *FEBS Letters*, 446:23–26, 1999.
- [40] Wydrzynski T. J. and Satoh K. *Photosystem II—The light-driven water:plastoquinone oxidoreductase*, volume 22, chapter 8, page 13. Springer, 2005.
- [41] D. A. Berthold, G. T. Babcock, and C. F. Yocum. a highly resolved, oxygen-evolving photosystem II preparation from spinach thylakoid membranes. *FEBS Letters*, 134:231–234, 1981.
- [42] W. Draber, K. Tietjen, J.F. Kluth, and A. Trebst. Herbicides in photosynthesis research. *Angew. Chem. Int. Ed. Engl.*, 30:1621–1633, 1991.
- [43] C. A. Tracewell and G. W. Brudvig. Characterization of the secondary electron-transfer pathway intermediates of photosystem II containing low-potential cytochrome *b559*. *Photosynthesis Research*, 98:188–197, 2008.
- [44] C. A. Buser, B. A. Diner, and G. W. Brudvig. Photooxidation of cytochrome *b559* in oxygen-evolving photosystem II. *Biochemistry*, 31:11449–11459, 1992.
- [45] D. H. Stewart and G. W. Brudvig. Cytochrome *b559* of photosystem II. *Biochimica et Biophysica Acta*, 1367:63–87, 1998.
- [46] A. Magnuson, M. Rova, F. Mamedov, P. O. Fredriksson, and S. Styring. The role of cytochrome *b559* and tyrosineD in protection against photoinhibition during in vivo photoactivation of photosystem II. *Biochimica et Biophysica Acta*, 1411:180–191, 1999.
- [47] Wydrzynski T. J. and Satoh K. *Photosystem II—The light-driven water:plastoquinone oxidoreductase*, volume 22, chapter 8, pages 188–193. Springer, 2005.
- [48] A. Trebst. The three-dimensional structure of the herbicide binding niche on the reaction center polypeptides of photosystem II. *Z. Naturforsch*, 42c:742–750, 1987.

- [49] C. Hansch and T. Fujita. A new substituent constant, PI , derived from partition coefficients. *Journal of the American Chemical Society*, 86:5175–5180, 1964.
- [50] G. Krishnan, Horst G. L., S. Darnell, and W. L. Powers. Growth and development of smooth bromgrass and tall fescue in TNT-contaminated soil. *Environmental Pollution*, 107:109–116, 2000.
- [51] P. Y. Robidoux, G. Bardai, L. Paquet, G. Ampleman, S. Thiboutot, J. Hawari, and G. I. Sunahara. Phytotoxicity of 2,4,6-trinitrotoluene (TNT) and octahydro-1,3,5,7-tetrazocine (HMX) in spiked arteficial and natural forest soils. *Arch Environ Contam Toxicol*, 44:198–209, 2003.
- [52] N. Boucher, L. Lorrain, and F. Bellemare. *Methode pour tester des activites photosynthetiques*.
- [53] D. I. Arnon. Copper enzymes in isolated chloroplasts polyphenoloxidase in beta vulgaris. *Plant Physiology*, 24(1):1–15, 1949.
- [54] P. J. Leeuwen, M. C. Nieveen, E. J. Meent, J. P. Dekker, and H. J. Gorkom. Rapid and simple isolation of pure photosystem ii core and reaction center particles from spinach. *Photosynthesis Research*, 28(3):149–153, 1991.
- [55] J. D. Brewster, A. R. Lightfield, and P. L. Bermel. Storage and immobilization of photosystem ii reaction centers used in an assay for herbicides. *Analytical Chemistry*, 67(7):1296–1299, 1995.
- [56] D. Laberge, R. Rouillon, and Carpentier R. Comparative study of thylakoid membranes sensitivity for herbicide detection after physical or chemical immobilization. *Enzyme and microbial technology*, 26(5-6):332–336, 2000.
- [57] C. Loranger and R. Carpentier. A fast bioassay for phytotoxicity measurement using immobilized photosynthetic membranes. *Biotechnology and Bioengineering*, 44(2):178–183, 1994.
- [58] K. Takashi, Usui H., D. Hobara, and Yamamoto M. Voltammetric properties of the reductive desorption of alkanethiol self-assembled monolayers from a metal surface. *Langmuir*, 18(13):5231–5238, 2002.
- [59] J. Wang. *Analytical electrochemistry*, page 29. John Wiley and Sons, 2006.

- [60] P. C. Meier and R. E. Zund. *Statistical methods in analytical chemistry*, pages 103–107. 1993.
- [61] E. Touloupakis, L. Giannoudi, S. A. Piletsky, L. Guzzella, F. Pozzoni, and M. T. Giardi. A multi-biosensor based on immobilized Photosystem II on screen-printed electrodes for the detection of herbicides in river water. *Biosensors and Bioelectronics*, 20(10):1984–1992, 2005.
- [62] F. Bettazzi, S. Laschi, and M. Mascini. One-shot screen-printed thylakoid membrane-based biosensor for the detection of photosynthetic inhibitors in discrete samples. *Analytica Chimica Acta*, 589(1):14–21, 2007.
- [63] K. Satoh, M. Oh-Hashi, Y. Kashino, and H. Koike. Mechanisms of electron flow through the Q_B site in photosystem II. *Plant Cell Physiology*, 36:597–605, 1995.
- [64] B. A. Diner and V. Petrouleas. Light-induced oxidation of the acceptor-side Fe(II) of Photosystem II by endogenous quinones acting through the Q_B binding site. II. Blockage by inhibitors and their effects on the Fe(III) EPR spectra. *Biochimica et Biophysica Acta*, 893:138–148, 1987.
- [65] K. Satoh, H. Koike, T. Ichimura, and S. Katoh. Binding affinities of benzoquinones to the Q_B site of Photosystem II in *Synechococcus* oxygen-evolving preparation. *Biochimica et Biophysica Acta*, 1102:45–52, 1992.
- [66] Y. Kashino, M. Yamashita, Y. Okamoto, H. Koike, and K. Satoh. Mechanisms of electron flow through the Q_B site in Photosystem II. 3. Effects of the presence of membrane structure on the redox reactions at the Q_B site. *Plant Cell Physiology*, 37:976–982, 1996.
- [67] J. Maly, C. Di Meo, M. De Francesco, A. Masci, J. Masojidek, M. Sugiura, A. Volpe, and R. Pilloton. Reversible immobilization of engineered molecules by Ni-NTA chelators. *Bioelectrochemistry*, 63(1-2):271–275, 2004.
- [68] J. Lu and Z. Zhang. A reusable optical sensing layer for picric acid based on the luminescence quenching of the Eu–thenoyltrifluoroacetone complex. *Analytica Chimica Acta*, 318:175C179, 1996.

- [69] G. He, H. Peng, M. Liu, T. and Yang, Y. Zhang, and Y. Fang. A novel picric acid film sensor via combination of the surface enrichment effect of chitosan films and the aggregation-induced emission effect of siloles. *Journal of Materials Chemistry*, 19(39):7347–7353, 2009.
- [70] O. Trott and A. J. Olson. Autodock vina: improving the speed and accuracy of docking with a new scoring function, efficient optimization and multithreading. *Journal of Computational Chemistry*, 31:455–461, 2010.
- [71] D. S. Goodsell, G. M. Morris, and A. J. Olson. Automated docking of flexible ligands: Applications of Autodock. *Journal of Molecular recognition*, 9:1–5, 1996.
- [72] A. Guskov, J. Kern, A. Gabdulkhakov, M. Broser, A. Zouni, and W. Saenger. Cyanobacterial photosystem II at 2.9Å resolution and the role of quinones, lipids, channels and chloride. *Nat. Struct. Mol. Biol.*, 16:334–342, 2009.
- [73] R. Takahashi, K. Hasegawa, A. Takano, and T. Noguchi. Structure and Binding Sites of Phenolic Herbicides in the Q_B Pocket of Photosystem II. *Biochemistry*, 49:5445–5454, 2010.
- [74] E. Haag, H. M. Gleiter, and G. Renger. Effects of photoinhibition on the PS II acceptor side including the endogenous high spin Fe²⁺ in thylakoids, PS II-membrane fragments and PS II core complexes . *Photosynthesis Research*, 31:113–126, 1992.